CHALMERS
UNIVERSITY OF TECHNOLOGY

3D Scanning of naturally corroded steel bars.

An assessment of corrosion behaviour and correlations to critical cross-sections.

Master's thesis in Concrete under Structural Engineering Division.

PRIYANKA DAS

DEPARTMENT OF ARCHITECTURE AND CIVIL ENGINEERING
DIVISION OF STRUCTURAL ENGINEERING

CHALMERS UNIVERSITY OF TECHNOLOGY
Gothenburg, Sweden 2025
www.chalmers.se

MASTER'S THESIS 2025

3D Scanning of naturally corroded steel bars.

An assessment of corrosion behaviour and correlations to Critical Cross-Sections.

Master's thesis work in the Master's Programme in Structural Engineering and Building Technology Division.

Priyanka Das

Department of Architecture and Civil Engineering

Division of Structural Engineering

Concrete Structures

CHALMERS UNIVERSITY OF TECHNOLOGY

Gothenburg, Sweden 2025

3D Scanning of naturally corroded steel bars

An assessment of corrosion behaviour and correlations to critical cross-sections

Priyanka Das

Master's Thesis 2025

Department of Architecture and Civil Engineering

Division of Structural Engineering

Concrete Structures

Chalmers University of Technology

SE -41296 Gothenburg, Sweden

PHONE: +46 (0)31-772 10 00

Cover:

Correlation between average corrosion degree and critical corroded parameters of steel bar specimen.

Chalmers repro- service / Dept. of Architecture and Civil Engineering

Gothenburg, Sweden, 2025

3D Scanning of naturally corroded steel bars

An assessment of corrosion behaviour and correlations to critical cross-sections

Master's thesis in the Master's Programme of Structural Engineering & Building Technology

Priyanka Das

Department of Architecture and Civil Engineering

Division of Structural Engineering

Concrete Structures

Chalmers University of Technology

Abstract

The present study focuses on the effect of corrosion of steel reinforcement in reinforced concrete (RC) structures. Corrosion has a large impact on the structural performance of RC structures. A cross-section reduction of the steel bar occurs due to the oxidation of steel which unequivocally convey a non-uniform distribution of pits along the bar length. For a specific length, it is possible to identify a critical cross-section (CCS), which attains the highest loss of area. This thesis defines CCS and illustrates how the different characterizing parameters of the same can be described from the measured average corrosion level of a specific bar length.

To cover this objective naturally corroded steel bars from a real bridge situated in Stallbacka were employed. After structural testing of the edge beams of the bridge, the steel reinforcement was extracted, cut into suitable lengths, and subsequently cleaned. Thereafter the average corrosion level of each specific bar was obtained by using two different techniques, gravimetric and 3D scanning. By weight loss method accurate measurements of the average corrosion level were obtained; by 3D scanning discrete corrosion level in each cross-section was quantified. In addition, variables such as pit depth, pit length, pit width, and, corroded perimeter, were measured from the CCS by combined physical and numerical post-processing of the 3D scanning techniques. These measurements led to a precise description of the CCS.

Finally, relations between all the measured parameters to the average corrosion level were obtained, hence possible predictions of the CCS from the estimated average corrosion level of a specific bar length could be described. Furthermore, in further works, the tensile properties of the utilized steel bars can be correlated to the CCS description and later estimate the reduction of capacity of the steel bars because of the presence of corrosion.

Keywords: Steel reinforcement, reinforced concrete structures, corrosion, structural performance, cross-section reduction, oxidation of steel, non-uniform distribution of pits, the highest loss of area, structural testing of the edge beams, average corrosion level, gravimetric and 3D scanning, pit depth, pit length, pit width and, corroded perimeter, post-processing, reduction of capacity of the steel bars

Table of contents:

Abstract ..... **i**
Contents ..... **ii**
List of Tables ..... **iii**
List of Figures ..... **iv**
Preface ..... **v**
Notations ..... **vi**
1. Introduction 1
1.1 Background 1
1.2 Aim 1
1.3 Methodology 2
1.4 Limitations 3
1.5 General Overview 4
2. Literature Review 5
2.1 General 5
2.2 Types of Corrosion in metal surface 5
2.3 Theoretical Background 8
2.4 Previous activity review 9
2.4.1 Mechanical Degradation due to Corrosion 9
2.4.2 Digital Technologies for Corrosion Assessment 10
2.4.3 Pit geometry and Statistical Modelling 11
2.4.4 Gap in Literature and Research Need 12
2.5 Present Research idea 13
3. Sampling and preparations 15
3.1 Reinforcement in Edge Beam 17
3.1.1 Geometrical Description 17
3.1.2 Chemical Composition 17
3.2 Cutting of Sample specimens 18
3.3 Cleaning bar specimens 18
3.4 Determination of weight loss 20
3.5 Optical measurement techniques 24
3.6 Summary 26
4. Post-processing using MATLAB 27
4.1 Steps for simulation progress 27
4.2 Corrosion level evaluation 27
4.3 Simulation Outcome: Average Corrosion degree 30
5. Evaluation of Present Study 32
5.1 Results Summary in Classification Learner 36
5.2 Discussion of findings 38
6. Response-Predictor Relations 39
7. Conclusion 44
References 46

List of Tables

Table 1: Specimen geometry and corrosion type

Table 2: Measured parameters and standard deviations describing the geometry of the ribbed reinforcement bar (in mm)

Table 3: Chemical composition of the steel rebar (values in %)

Table 4: Computed weight-loss percentages of all specimens representing average corrosion degrees, used for comparison with localized corrosion obtained from 3D scanning

Table 5: Average corrosion from computer simulations

Table 6: Specimen geometry and simulated critical corrosion parameters

Table 7: Average and maximum corrosion degree with normalized pit geometry parameters

Table 8: Classification Results (Gravimetric average corrosion as Response)

Table 9: Classification Results (Simulation based average Corrosion as Response)

List of Figures

Figure 1: Overview of the thesis scope and research framework
Figure 2: Uniform corrosion in a steel reinforcement rebar
Figure 3: Pitting corrosion on a steel surface
Figure 4: Crevice corrosion in air-tied seal between two pipes
Figure 5: Intergranular corrosion in an aircraft component
Figure 6: Galvanic corrosion in steel plate due to the presence of copper in a salt water electrolyte
Figure 7: Stress corrosion cracking in a metal surface
Figure 8: Experimentally tested corroded steel rebar with skewed and straight rib
Figure 9: Geometry of ribbed reinforcement bars
Figure 10: Horizontal Band Saw cutting machine
Figure 11: Surface cleaning process- metallic brushing, sandblasting & acid immersion (top to bottom)
Figure 12: Sandblasting Cabinet
Figure 13: Experimental setup showing the steel frame and 3D scanning device
Figure 14: 3D surface model generated from VX element
Figure 15: A general view of a corroded specimen with VX element scan results
Figure 16: 3D Polygon mesh representation in Geomagic Wrap
Figure 17: Conversion of polygon mesh into a point cloud in Geomagic Wrap
Figure 18: Overview of the method for determining corrosion percentage variations along a bar specimen
Figure 19: Cross-sectional area values(blue) and best-fit curve(red) plotted along the bar length (xx)
Figure 20: Best-fit cross-sectional areas (qq2) along the length of the steel bar specimen (xx)
Figure 21: Normalized cross-sectional area values plotted along the bar length(xx)
Figure 22: Pit width in relation to average corrosion degree
Figure 23: Pit depth compared with average corrosion degree
Figure 24: Corrosion level at the critical cross-section (CCS) for varying average corrosion
Figure 25: Diameter reduction ratio (d/d_0) with increasing average corrosion
Figure 26: Normalized pit depth (p_{depth}/d_0) across corrosion levels
Figure 27: Normalized pit width (p_{width}/d_0) as corrosion progresses
Figure 28: Normalized pit length (p_{length}/d_0) versus corrosion degree
Figure 29: Reduction of normalized critical perimeter (P_{crit}/P_0) due to corrosion progression
Figure 30: Ratio of perimeter reduction to area reduction (P_r/A_r) across corrosion levels

Preface

This thesis was conducted as part of the research work within the Structural Engineering division at Chalmers University of Technology. The study aims to establish a correlation between average corrosion levels and the most critically affected cross-sections of naturally corroded steel reinforcement, extracted from a real Swedish bridge girder located in Stallbacka. This investigation is expected to contribute to the foundation for future research into the mechanical behavior of corroded reinforcement bars and their implications for structural integrity.

The anchorage of the bridge deck plays a vital role in structural performance. Unfortunately, the reinforcement bars extracted for this study exhibited significant degradation due to prolonged exposure and corrosion, leading to a substantial reduction in their anchorage capacity. In this context, the research focused on identifying the critical cross-sections, the areas with the highest loss of cross-sectional area and examining their relationship with the average corrosion degree along the bar length.

To achieve this, advanced 3D scanning technology was employed to generate high-resolution, three-dimensional models of the corroded bars. Complementary laboratory testing and simulation work were also carried out using modern testing facilities. These provided additional data for analyzing pit characteristics such as depth, length, width, and corroded perimeter.

Moreover, machine learning techniques were explored to classify data obtained from manual measurements and simulations. Although the predictive capabilities regarding average corrosion degree were limited, the use of machine learning offered valuable insights into model performance and data classification.

I would like to express my sincere gratitude to my supervisor, Ignasi Fernandez Perez, for his continuous support, insightful feedback, and invaluable guidance throughout the course of this research.

It is my hope that this thesis serves not only as a contribution to the academic discourse on corrosion assessment but also as a useful reference for future students and researchers within the Structural Engineering division at Chalmers University of Technology.

Gothenburg, 2025

Priyanka Das

Notations

All variables used in the report are presented alphabetically.

Roman Uppercase Letters

Symbol	Description
A_0	Cross-sectional area of the uncorroded bar
A_{crit}	Critical cross-sectional area of the bar specimen
A_r	Ratio of critical to uncorroded cross-sectional area, A_{crit}/A_0
CS 1	Cross-section 1 in critical locations
CS 2	Cross-section 2 in critical locations
CS 3	Cross-section 3 in critical locations
P_0	General perimeter of the bar
P_{crit}	Critical perimeter
P_r	Ratio of critical to general bar perimeter

Roman Lowercase Letters

Symbol	Description
d	Diameter of uniformly corroded bar
d_0	Original diameter of the uncorroded bar
p_{length}	Pit length
p_{width}	Pit width
p_{depth}	Pit depth
q	Cross-sectional area of the steel bar specimen along its length
qq2	Best-fit cross-sectional area values of the steel bar
w	Weight of the uncorroded bar
w_{cor}	Weight of the corroded bar

1 Introduction

1.1 Background

Steel reinforcement in concrete is primarily employed to resist tensile stresses, but its susceptibility to corrosion significantly compromises the durability and longevity of reinforced concrete (RC) structures. As corrosion progresses, it not only affects the structural serviceability, manifesting as cracking or spalling of the concrete cover, but also undermines structural safety by reducing the load-carrying capacity of RC members.

As the corrosion of steel bars is predominately an electrochemical process, it involves a series of oxidation reactions. These reactions occur simultaneously at anodic and cathodic sites on the reinforcement surface, where ferrous ions are oxidized to form ferrous hydroxide, which subsequently transforms into hydrated ferric oxide, commonly known as rust. This transformation leads to a loss of metallic iron and an increase in volume, which can adversely affect the mechanical properties of the reinforcing steel, including its strength and ductility.

Previous research has extensively assessed the mechanisms of corrosion and its effects on the bond between steel and concrete. Several studies have also demonstrated the impact of corrosion on the mechanical properties of reinforcing bars, particularly the decline in yield stress with increasing levels of corrosion.

The current thesis investigates the average corrosion degree of naturally corroded steel bars extracted from the edge beams of the Stallbacka Bridge. As corrosion progresses, certain regions of the reinforcement may deteriorate more severely than others, forming critical cross-sections**,** the locations with the highest material loss. This study aims to identify and characterize these critical sections and to establish correlations between their defining parameters and the average corrosion level of the entire bar.

To achieve this, a 3D scanning technique was employed to generate detailed surface models of the corroded bars. The scanned data were used in simulations and post-processing analyses to quantify geometric features such as pit depth, width, and length in the most severely corroded areas. These parameters were then analyzed in relation to the average corrosion degree, in order to develop predictive relationships and contribute to a better understanding of how uniform and localized corrosion affect overall bar performance.

1.2 Aim

This study focuses on analyzing and delineating the Critical Cross-Section (CCS) in naturally corroded reinforcing steel bars, while examining the correlation between CCS parameters and the measured average corrosion. To achieve this, the study seeks to:

- Determine the average corrosion level of each bar using both gravimetric analysis and high-resolution 3D scanning.
- Identify the critical cross-section (CCS) along each bar, where the maximum local corrosion and most severe geometric degradation occur.
- Quantify the CCS geometric parameters, including pit depth, length, width and corroded perimeter.

- Investigate how average corrosion levels relate to CCS parameters to predict critical cross-sectional losses caused by corrosion.

By achieving these objectives, this research lays the groundwork for future studies that aim to correlate CCS characteristics with the mechanical properties of corroded steel bars, enabling the estimation of reductions in tensile capacity due to corrosion and improving predictive modeling of structural degradation in aging RC structures.

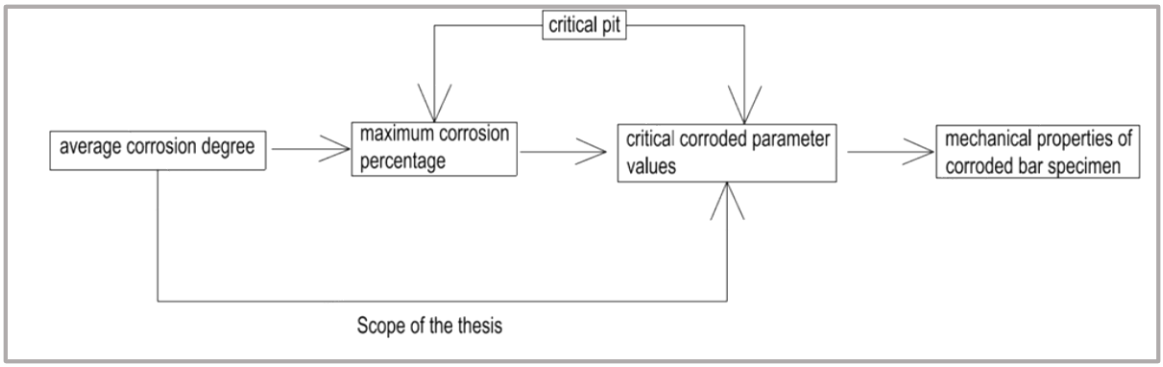

Figure 1: Overview of the thesis scope and research framework

This diagram (Figure 1), illustrates the methodological framework of the study. The average corrosion degree, determined using both gravimetric analysis and 3D scanning, is correlated with the maximum corrosion percentage obtained from the scanned data. These values help locate the critical pit, from which corroded geometric parameters such as pit depth, width and perimeter are extracted. These parameters form the basis for estimating the mechanical properties of corroded bar specimens in future studies.

1.3 Methodology

This research was structured into three different phases:

Phase 1: Specimen Preparation
The initial phase involved the selection and preparation of naturally corroded steel reinforcement bars extracted from the edge beams of the Stallbacka Bridge. Bars were chosen based on visual assessment to ensure a representative range of corrosion levels. The specimens exhibited varying degrees of corrosion, with rust and remnants of concrete adhering to the surface. These were carefully cleaned to remove corrosion products and concrete residues, allowing accurate evaluation of the bar's physical condition.

Phase 2: 3D Scanning
In the second phase, the cleaned specimens were scanned using a 3D laser scanner available at the Structural Engineering Laboratory at Chalmers University of Technology. The scanning process involved careful marking and systematic documentation of each bar to ensure consistency and repeatability in capturing surface details and pit geometry.

Phase 3: Data Analysis and Correlation
In this phase, the collected data were analyzed to establish key relationships between corrosion matrices. The overall corrosion level of each bar was determined through

gravimetric weight-loss measurements, while detailed local corrosion patterns were captured using 3D scanning. The CCS, representing the region of most severe localized degradation, was examined using both scanning data and manual observations.

The findings were employed to link average corrosion levels with local corrosion features and pit geometry, offering insight into how corrosion influences the structural performance of reinforcing steel.

1.4 Limitations

The initial objective of this research was to predict critical corrosion levels based on the corresponding average corrosion degrees. While critical values were manually measured from each steel bar specimen, several limitations affected the accuracy and reliability of these results.

Firstly, due to time constraints, pit dimensions, such as depth, width, and length were measured manually using slide calipers. This approach introduced potential human and instrumental errors, affecting the precision of the collected data.

Secondly, machine learning techniques were applied to predict critical corrosion values from the measured average corrosion levels. However, the results obtained from the classification models showed limited accuracy and could not be deemed reliable for conclusive predictions. It is likely that alternative modeling techniques or more comprehensive datasets are necessary to enhance predictive performance.

These limitations indicate that while the correlations established in this study provide a meaningful basis, further work is needed to improve prediction reliability and develop a more robust methodology for estimating critical corrosion characteristics from average measurements.

1.5 General Overview

This thesis is categorized into the following chapters:

- **Chapter 2** provides a concise review of previous studies on steel corrosion in reinforced concrete, highlighting how earlier research has shaped the motivation, methodology and objectives of the present work.

- **Chapter 3** details the preparation of naturally corroded bar specimens, including cutting to appropriate lengths and cleaning via abrasive sandblasting. It also outlines the 3D scanning process used to capture surface geometries, producing high-resolution polygon mesh and pint cloud models for further analysis.

- **Chapter 4** focuses on post-processing the 3D scanned data and performing simulation analyses to quantify corrosion in steel bars. The chapter details the identification of critical corrosion sections and the calculation of key parameters, including pit dimensions and both maximum and average corrosion percentages.

- **Chapter 5** presents the results derived from the processed data, including manually recorded measurements and simulation outputs. It also explores the use of the Classification Learner tool to assess how well average corrosion degrees predict critical cross-section parameters.

- **Chapter 6** describes the relationships between critical corrosion parameters and the average corrosion degree, forming the core analytical component of the study.

- **Chapter 7** summarizes the main findings and discusses their overall significance, emphasizing how the identified relationships between average corrosion degree and critical geometric parameters improve the understanding of corrosion effects on reinforcing steel.

2 Literature Review

2.1 General

Steel is the primary reinforcement material in concrete because of its high tensile strength and ductility. The bond between steel and concrete is essential for reinforced concrete (RC) members, enabling steel to resist the tensile forces that concrete cannot. Environmental factors such as moisture, temperature changes, and chloride ingress can cause corrosion over time, reducing material properties and structural integrity.

The flexural and tensile strength of reinforced concrete members is greatly influenced by the corrosion of steel rebar. Corrosion reduces the cross-sectional area of the rebar, thereby weakening its load-bearing capacity. Moreover, as the corrosion progresses, it generates expansive products that exert internal pressures on the surrounding concrete, potentially leading to cracking, spalling, and a loss of bond strength between the steel and concrete. These issues, if left unaddressed, can compromise the safety and longevity of structures.

This research quantifies corrosion severity and examines the relationship between average corrosion levels and critical local damage. The methodology combines manual measurements, high-resolution 3D scanning, and machine learning. By linking average and maximum corrosion, the study aims to enhance predictive assessment of deterioration, supporting better estimates of service life and maintenance planning for RC structures.

2.2 Types of Corrosion on metal surface

Corrosion of steel reinforcement in concrete is a multifaceted process influenced by several parameters; environmental exposure, material composition and concrete quality. Through these corrosion mechanisms, steel rebars got effected in different ways. A proper understanding of these corrosion types helps in interpreting 3D scans, identifying critical cross-sections, and evaluating structural durability. The main corrosion mechanisms affecting reinforcing steel in concrete are described below.

1. Uniform Corrosion

Uniform corrosion is one of the most frequently observed forms of damage in steel reinforcement, and it tends to be less critical than localized corrosion types. It occurs when the passive oxide film on the steel surface deteriorates uniformly, often due to carbonation or prolonged exposure to mildly aggressive environments. The resulting even reduction in diameter causes predictable material loss and is relatively easier to quantify and manage. For instance, in bridge structures exposed to de-icing salts in Sweden, uniform corrosion has been observed as a consistent thinning of rebar cross-sections (Bamforth,2002).

Figure 2: Uniform corrosion in a steel reinforcement rebar

2. Pitting Corrosion

Pitting corrosion is a localized form of corrosion where small, deep pits form on the metal surface due to the breakdown of the protective oxide film or coating. This is one of the most destructive types of corrosion because pits can penetrate deeply into the material, weakening the steel and leading to rapid structural failure. Pitting corrosion is particularly hard to predict, detect, and characterize. Once initiated, pits can grow into irregular cavities with varying shapes and sizes, which complicates damage assessment. Pitting can also be initiated by localized damage to the protective coating or by non-uniformity in the metal structure.

Figure 3: Pitting corrosion on a steel surface

3. Crevice Corrosion

Crevice corrosion occurs in localized regions where a stagnant micro environment is created, often due to the presence of dirt, sand deposits, or the design of the steel component (e.g., under bolts or rebar heads). This corrosion is driven by a difference in ion concentration between the crevice and the surrounding area, resulting in a corrosion cell. The environment inside the crevice is typically low in oxygen, which facilitates the corrosion process, while the unshielded surface acts as the cathode. In high-chloride, acidic environments, this type of corrosion is more pronounced, leading to accelerated damage in areas with poor exposure to air or water flow.

Figure 4: Crevice corrosion in air-tied seal between two pipes

4. Inter-granular Corrosion

Inter-granular corrosion is a localized form of corrosion that occurs at the grain boundaries of a metal, where the microstructure exhibits distinct grain boundaries that separate individual grains of metal. Impurities or alloying element depletion/enrichment at these grain boundaries can initiate corrosion along these lines, leaving the bulk of the metal largely intact. This type of corrosion can compromise the integrity of the steel, especially in environments with elevated temperatures or high concentrations of corrosive agents, such as acids or chloride-rich environments.

Figure 5: Intergranular corrosion in an aircraft component

5. Galvanic Corrosion

Galvanic corrosion happens when two electrochemically dissimilar metals are in direct electrical contact in the presence of an electrolyte. The difference in electrochemical potentials between the two metals creates a corrosion cell, where one metal acting as the anode and the other as the cathode. This can accelerate the degradation of the more anodic material, often resulting to significant localized corrosion. To mitigate galvanic corrosion,

materials with similar electrochemical potentials should be selected, and care should be taken to avoid direct contact between dissimilar metals in corrosive environments.

Figure 6: Galvanic corrosion in steel plate due to the presence of copper in a salt water electrolyte

6. Stress Corrosion Cracking (SCC)

Stress corrosion cracking (SCC) is a type of cracking that occurs due to the combined effects of tensile stress and a corrosive environment, typically at elevated temperatures. This corrosion mechanism is particularly dangerous because it can cause sudden and catastrophic failure of the material, even though the visible damage may be minimal. SCC is difficult to detect since the majority of the steel surface remains intact, with only fine cracks appearing in the micro-structure. The presence of external stress, such as tensile loads, along with residual stresses from manufacturing processes (e.g., welding, grinding), can exacerbate SCC. Proper material selection and environmental control are critical in mitigating the risk of SCC.

Figure 7: Stress corrosion cracking in a metal surface

2.3 Theoretical Background

The corrosion of steel reinforcement in concrete structures has been extensively studied due to its significant impact on structural performance. Key consequences of corrosion include loss of bond between steel and concrete, cracking of the concrete cover, reduction in

anchorage capacity, and diminished load-bearing capacity. From a local perspective, researchers have also investigated how corrosion pit distribution influences the mechanical properties of reinforcing bars. However, earlier studies often relied on manual methods to describe these localized effects due to technical limitations.

Advancements in photogrammetry and digital scanning technologies have recently made it possible to digitally capture and analyze the surface conditions of corroded steel bars with high accuracy. Various scanning techniques have been employed in the literature to model and assess pit distribution and pit geometry [3.5]. These technologies enable detailed post-processing to quantify corrosion along the length of the bar. With such data, it becomes feasible to simulate the tensile behavior of corroded bars using three-dimensional finite element (3D FEM) modeling, thereby deepening our understanding of how localized corrosion affects structural performance [see Chapter 4].

Corrosion of reinforcement causes a premature degradation in reinforced concrete structures. Among its effects, the elongation capacity of steel bars is particularly compromised, increasing the risk of brittle failure. Both the residual ultimate tensile strength and ductility of the steel are significantly reduced in corroded bars compared to their uncorroded counterparts.

In assessing the structural performance of corroded elements, the most deteriorated or critical locations of the bars become especially important. In this context, parameters such as perimeter reduction, loss of cross-sectional area, and diameter reduction at severely pitted sections are valuable indicators. This study aims to correlate these critical-section parameters with the average corrosion degree of each specimen. Establishing such relationships may allow for predictive modeling, enabling the estimation of maximum corrosion-induced losses based solely on average corrosion levels.

To define corrosion levels on an average basis, both gravimetric and 3D scanning techniques were used. The gravimetric method, which involves measuring mass loss due to corrosion, provides a quick and reliable estimation of the average corrosion degree. Meanwhile, 3D scanning captures geometric data across the bar surface, generating polygon meshes and converting them into point clouds for further analysis and simulation. This dual approach enables both global (average) and local (critical) assessment of corrosion damage.

Manual data collection was also carried out to characterize pit geometry (pit length, width, and depth) at the most critical locations. A machine learning classifier; specifically, a classification learner was employed to assess whether these pit characteristics could be predicted based on the average corrosion degree. Nonetheless, the relationship between the average corrosion level and geometric parameters at critical sections remains a promising pathway for evaluating and predicting structural degradation in naturally corroded specimens.

2.4 Previous activity review

2.4.1 Mechanical Degradation due to Corrosion

Corrosion significantly affects the mechanical performance of steel reinforcement in concrete structures. As the protective passive layer around steel breaks down due to carbonation or chloride ingress, the steel begins to lose mass, cross-sectional area, and mechanical integrity.

This degradation impacts key mechanical properties such as tensile strength, ductility, fatigue life, and bond performance with the surrounding concrete.

Several studies have explored the influence of corrosion on the stress–strain behavior and ultimate strength of reinforcing bars. Fernández, Bairán, and Marí (2016) developed a 3D finite element model of corroded steel bars using realistic pit geometries obtained from experimental 3D optical scans. Their study highlighted how the shape, depth and distribution of corrosion pits influence the stress-strain response and local failure mechanisms of the bars, providing a more detailed understanding of mechanical degradation due to corrosion (Construction and Building Materials, 124, 519-532).

Similarly, Zhang et al. (2012) conducted tensile and fatigue tests on rebars subjected to various levels of corrosion. Their findings indicated a significant reduction in both ultimate tensile strength and fatigue resistance as corrosion levels increased, pointing to a critical relationship between material loss and failure risk (Construction and Building Materials, 34, 409–417).

Apostolopoulos (2007) investigated the behavior of S500s reinforcement bars under low-cycle fatigue loading. His results revealed that corrosion sharply reduced the energy absorption capacity of the bars, which is especially concerning in seismic applications where repeated stress cycling occurs (Construction and Building Materials, 21(7), 1447–1456).

Further studies have also considered combined effects. For instance, Xiong et al. (2017) investigated how elevated temperature, when combined with corrosion damage, can accelerate the degradation of mechanical properties. This is particularly relevant for structures exposed to both harsh environmental and fire conditions. In a different context, Xu (2015) examined how static loading coupled with carbonation accelerates the deterioration of tensile performance in corroded steel (Materials, 8(12), 8561–8577).

These findings collectively demonstrate that corrosion is not merely a mass loss phenomenon but a complex process that significantly alters the stress response, failure mode, and safety margin of reinforcement bars. As a result, accurate mechanical assessment becomes increasingly difficult as corrosion advances, particularly when localized damage such as pitting is involved.

While these mechanical studies have contributed significantly to understanding the consequences of corrosion, most focus on artificially induced corrosion under laboratory-controlled conditions. In contrast, the present research draws from naturally corroded specimens and does not directly assess mechanical properties. Instead, it focuses on identifying critical geometric damage through 3D scanning, which provides an alternative pathway for evaluating structural reliability. Geometric assessment is a valid and necessary alternative, particularly for naturally corroded specimens, because it allows for a direct examination of the actual degradation patterns that occur in field conditions. This approach can offer insights into localized damage and its potential impact on structural integrity, which mechanical testing may not fully capture, thus strengthening the research rationale.

2.4.2 Digital Technologies for Corrosion Assessment

In recent years, the advancement of digital technologies has significantly enhanced the precision and efficiency of corrosion assessment in reinforced concrete structures. Traditional

methods such as visual inspection, weight loss measurement, and manual dimensioning (e.g., with slide calipers) often suffer from limitations related to subjectivity, low resolution, or access to embedded reinforcement. As a result, researchers and engineers have increasingly turned to non-contact, high-resolution digital scanning techniques to analyze corrosion-induced damage with greater accuracy.

Optical techniques such as photogrammetry, structured-light or stereo-camera scanning have been used to reconstruct the real surface morphology of corroded reinforcement, generating dense point clouds and high-resolution polygonal meshes that capture realistic corrosion patterns. For example, Fernández, Lundgren, and Zandi (2018) used a stereo optical 3D measurement system to reconstruct corroded steel bars, allowing accurate quantification of pit geometry, cross-sectional loss, and spatial corrosion distribution. Their results demonstrated that digital methods can capture finer details than conventional cleaning or gravimetric approaches, especially for irregular corrosion patterns.

Digital models generated from scanning can also be integrated into computational simulations. Once the 3D geometry is captured, it can be imported into finite element (FE) software to analyze localized stress-strain behaviour or evaluate the influence of actual pit geometries on tensile performance. For example, Zeng et al. (2022) developed a finite element modeling method for corroded steel structures with randomly distributed pitting, showing that even small variations in pit size or location can lead to significant changes in mechanical response. Such approaches highlight the growing role of digital technologies not only for inspection but also as inputs for predictive modeling.

Long-term corrosion effects in naturally aged bars have also been studied using these digital tools. Fernández and Berrocal (2019) investigated 30-year-old naturally corroded reinforcing bars and found that localized pitting and irregular cross-sectional loss significantly reduced ductility and ultimate strain, even when average cross-sectional reductions were moderate. By combining traditional gravimetric measurements with 3D scanning, they could map corrosion damage more accurately and relate it to tensile performance. Their study emphasizes that conventional methods alone may underestimate the structural vulnerability of aged reinforcement, underlining the importance of high-resolution digital evaluation in real-world applications.

Despite their advantages, digital technologies still face challenges, particularly with scanning small-diameter rebars, dealing with occlusions, and handling surface reflections from rust. Furthermore, integrating scanned data into predictive models remains complex due to the irregular and stochastic nature of natural corrosion. Nonetheless, the growing accessibility and resolution of 3D scanners, combined with processing tools like point cloud software and mesh editing platforms, are steadily making digital assessment the preferred method in research and, increasingly, in field applications.

In the present study, a high-resolution 3D structured light scanner was used to assess corrosion on naturally aged rebars. This allowed for accurate geometry capture, including pit distribution and critical section loss, and the data was later used for both visual analysis and computer simulations to determine maximum corrosion levels. This digital workflow represents a shift from conventional evaluation methods toward a more comprehensive and data-rich approach to understanding corrosion damage.

2.4.3 Pit geometry and Statistical Modeling

The geometry of corrosion pits; especially pit depth, cross-sectional loss at critical sections, and the distribution of localized corrosion plays a decisive role in the residual mechanical capacity of steel reinforcement. Unlike uniform corrosion, which can often be approximated by average mass loss or diameter reduction, pitting corrosion leads to localized reduction of cross-section and stress concentrations that may significantly compromise load-bearing capacity and ductility.

A widely cited modelling study by Fernández, Bairán, and Marí (2016) developed a fiber-section model that integrates pit geometry, localized losses, and non-uniform material distribution to produce stress–strain (σ–ε) and fatigue curves for corroded rebars. Their results show that local pits, even when mass loss is modest, can drastically degrade mechanical performance, underscoring the disproportionate impact of pit severity compared to average corrosion degree.

Experimental evidence further supports the significance of pit morphology. In their 2015 study, the same authors conducted tens of monotonic and cyclic tensile/fatigue tests on artificially corroded bars, along with careful pit characterization in the critical cross-section. Their findings confirm a severe nonlinear reduction in ductility and fatigue life associated with corrosion degree and pit geometry.

Recently, non-uniform corrosion patterns have been studied using advanced imaging, for example, 3D reconstruction via CT scanning, revealing that natural corrosion rarely distributes uniformly around the bar. A 2025 investigation demonstrated significant variation longitudinally and circumferentially, with deeper pits occurring near concrete cracks or edges.

These developments underline the limits of relying solely on average metrics (like mass loss or nominal diameter reduction) to assess corrosion damage. Statistical or probabilistic modeling; informed by high-resolution geometric data, becomes essential to capture variability in pit depth, spacing, and distribution, and to predict structural risk more realistically.

Given the scarcity of data on naturally corroded bars with detailed geometric mapping, there remains a strong need for expanded datasets combining high-resolution scans (or CT), manual measurements, and mechanical testing, to calibrate predictive models that can estimate performance from visible corrosion indicators.

2.4.4 Gap in Literature and Research Need

Although extensive work has been done on the mechanical degradation of corroded rebars and the use of digital tools for corrosion quantification, several important research gaps remain. Firstly, most studies have emphasized either mechanical testing or digital inspection, but very few have integrated the two in a way that bridges local damage indicators (like pit depth) with global corrosion parameters (like average mass loss).

Secondly, the majority of experimental studies uses artificially corroded specimens, which tend to produce more uniform, predictable damage patterns. This limits the applicability of the findings to real-life structures, where natural corrosion is irregular, often influenced by environmental factors like moisture, chlorides, carbonation, and temperature variation. Thus, conclusions drawn from controlled lab corrosion may not fully translate to in-situ behavior.

Moreover, while digital scanning has established a new benchmark for geometric data acquisition, its potential is still largely untapped in predictive modeling. Only a limited number of studies have explored the quantitative relationships between average corrosion degree and extreme geometrical loss, an essential consideration for field engineers aiming to evaluate structural safety using limited information. In addition, the application of machine learning techniques for predicting pit geometry or identifying critical cross-sections remains relatively underexplored, primarily due to the scarcity of high-quality corrosion datasets.

Finally, the influence of critical corrosion sections on simulation-based structural evaluation is under-represented in current literature. This is significant because engineering decisions are often based on worst-case scenarios, which require identifying and analyzing the most severely affected regions of the reinforcement.

The present research addresses these gaps by:

- Using naturally corroded rebars, enhancing field relevance.
- Applying 3D scanning to define true pit geometry with high resolution.
- Attempting to develop a predictive relationship between average corrosion levels and critical cross-sectional damage.
- Exploring the use of manual measurements and simulations as a hybrid approach.
- Highlighting the limitations of current modeling and proposing directions for future improvement.

2.5 Present Research idea

Building upon the limitations identified in earlier studies, this research proposes a new methodology aimed at bridging the gap between global and localized corrosion assessment. While previous works have predominantly emphasized the degradation of mechanical properties, such as tensile strength, fatigue life, and bond performance, few have explored the relationship between average corrosion degree and critical geometric losses observed at the most deteriorated cross-sections.

The motivation for this research stems from the need for a more predictive and field-relevant model. Traditional gravimetric techniques provide average corrosion degree, a global indicator that reflects overall material loss. However, such averages often fail to capture the most critical localized damage, especially in cases involving pitting corrosion, where structural performance is governed by extreme loss in small sections.

This study introduces a dual approach involving manual measurement and high-resolution 3D scanning to analyze the corrosion profiles of naturally corroded steel rebars. Initially, critical pit dimensions, depth, length, and width were measured by hand using a Vernier caliper. While this method allowed for targeted measurement at visually degraded sections, the nearly circular geometry of rebars and limitations in tool accuracy introduced a degree of measurement uncertainty.

To overcome these limitations, a structured light 3D scanner was used to digitally capture the complete geometry of each rebar specimen. The scanning process produced detailed surface

reconstructions, allowing precise extraction of geometric parameters such as maximum diameter reduction, cross-sectional area loss, and pit distribution along the bar. The resulting detailed digital models were then used in computer simulations to determine the maximum corrosion percentages along the length of each specimen.

Although the simulations provided sufficient information to identify the most corroded regions, manual pit measurements were retained for comparative analysis. The intent was to explore whether predictive relationships could be established between average corrosion degree and extreme geometric losses, thereby offering engineers a more practical tool for estimating worst-case scenarios using average data alone.

To this end, a classification learner from a supervised machine learning toolkit was employed to test whether critical corrosion indicators could be predicted based on average mass loss. Although the model's predictive accuracy was limited, likely due to data set size and natural variability, the exercise highlighted a promising research direction for future studies.

In summary, this research presents a geometry-centered framework for evaluating corrosion in reinforcement bars. By focusing on naturally corroded specimens, incorporating both manual and digital measurements, and attempting predictive modeling of critical losses, the study offers a novel contribution to the field of structural durability assessment. These findings provide practical applications by informing field assessments and maintenance planning. By correlating average corrosion parameters with critical geometric losses, engineers can estimate worst-case scenarios, facilitating proactive maintenance strategies. Moreover, this research could potentially influence engineering standards, ensuring that they reflect the effects of natural corrosion patterns on reinforcement durability.

3 Sampling and preparations

The specimens used in this study were part of a larger experimental campaign conducted at Chalmers University of Technology. They were extracted from the edge beams of the Stallbackabron Bridge in Sweden during repair works after approximately 30 years of natural exposure to chloride-induced corrosion from de-icing salts. In a previous phase of this campaign, four-point bending tests were carried out to investigate the anchorage failure in corroded beams.

From these beams, thirty-nine steel rebar specimens were prepared, categorized as long specimens (~400 mm) and short specimens (~300 mm). Figure 8 shows representative examples of rebars with skewed and straight ribs.

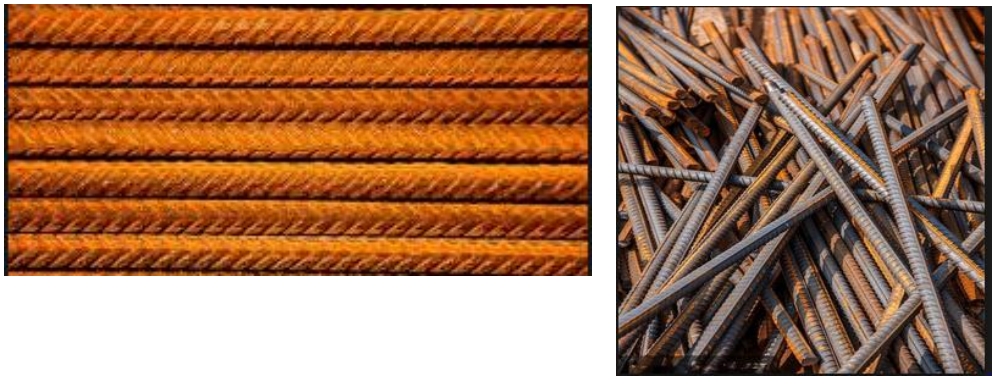

Figure 8: Experimentally tested corroded steel rebar with skewed and straight rib

Table 1 provides an overview of all specimens and their corrosion characteristics. Two complementary methods were applied to determine corrosion loss:

- the gravimetric method, to measure overall(average) corrosion from weight loss, and
- 3D scanning and computer simulations, to capture detailed surface geometry and local corrosion variations.

These two datasets were later correlated to establish relationships between average corrosion and critical cross-sectional degradation.

Table 1, Specimen geometry and corrosion type

Specimen #	Specimen length(mm)	Rib Type	Corrosion Status	Type of Corrosion
1	410	Skewed	Corroded	Uniform
2	410	Skewed	Corroded	Uniform
3	400	Skewed	Corroded	Uniform
4	400	Skewed	Corroded	Uniform
5	400	Skewed	Corroded	Uniform
6	400	Skewed	Corroded	Uniform
7	400	Skewed	Corroded	Uniform
8	415	Skewed	Corroded	Uniform
9	410	Skewed	Corroded	Uniform
10	400	Skewed	Corroded	Uniform
11	410	Skewed	Corroded	Uniform
12	400	Skewed	Corroded	Uniform
13	410	Skewed	Corroded	Uniform
14	400	Skewed	Corroded	Uniform
15	400	Skewed	Corroded	Uniform
16	410	Skewed	Corroded	Uniform
17	400	Skewed	Corroded	Uniform
18	400	Skewed	Corroded	Uniform
19	400	Skewed	Corroded	Uniform
20	300	Straight	Corroded	Uniform
21	300	Straight	Corroded	Uniform
22	310	Straight	Corroded	Uniform
23	300	Straight	Corroded	Uniform
24	300	Straight	Corroded	Uniform
25	300	Straight	Corroded	Uniform
26	300	Straight	Corroded	Uniform
27	300	Straight	Corroded	Uniform
28	300	Straight	Corroded	Uniform
29	300	Straight	Corroded	Uniform
30	300	Straight	Corroded	Uniform
31	310	Straight	Corroded	Uniform
32	300	Straight	Corroded	Uniform
33	300	Straight	Corroded	Uniform
34	300	Straight	Corroded	Uniform
35	305	Straight	Corroded	Uniform
36	305	Straight	Corroded	Uniform
37	300	Straight	Corroded	Uniform
38	300	Straight	Corroded	Uniform
39	300	Straight	Corroded	Uniform

3.1 Reinforcement in Edge Beam

Steel rebars were carefully extracted from the edge beams of Stallbackabron Bridge edge beams. The diameter of the tensile reinforcement was 16 mm, and two different rib geometries, skewed and straight were observed, both corresponding to steel class Ks60.

3.1.1 General Description

Each rebar was cut into lengths of approximately 400 mm or 300 mm, selected to suit subsequent testing and tensile requirements. Dimensional measurements were taken using a vernier caliper with a resolution of 10 μm (figure 9 and table 2), with values representing the average of multiple readings.

Figure 9: Geometry of ribbed reinforcement bars

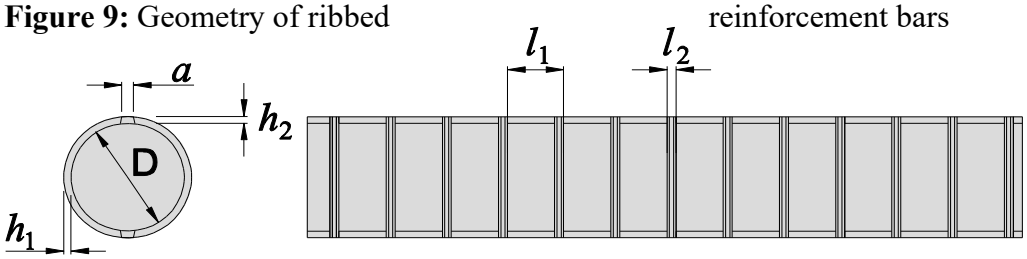

Table 2.

Measured parameters and standard deviations describing the geometry of the ribbed reinforcement bar (in mm)

Steel class	Nominal diameter	D	σ	a	σ	h_1	σ	h_2	σ	l_1	σ	l_2	σ	θ (º)
Ks60	Ø16	15.7	0.03	1.91	0.02	1.23	0.1	1.23	0.1	9	0.36	2.27	0.1	90

3.1.2 Chemical composition

The chemical composition of the extracted steel specimen was investigated by using Scanning Electron Microscopy (SEM). The values presented correspond to the average values obtained for each component in different scanning points throughout the bar cross-section.

Table 3.

Chemical composition of the steel rebar (values in %)

	C	**O**	**Si**	**Mn**	**Cr**	**Ni**	**Cu**
Ks60	2.84	4.63	0.22	1.08	0.19	0.17	0.51

3.2 Cutting of Sample specimens

Figure 10: Horizontal Band Saw cutting machine

The machine, Horizontal Band Saw (Figure 10), was used for cutting all corroded steel rebar. The normal speed of the machine is 5 revolutions per minute. During cutting there was a continuous flow of cold water so to make cutting in cold conditions by the blade. Steel bars were placed perpendicularly to the blade and a gap of a minimum of 25 mm between the blade and specimen was maintained while starting the machine. All bars were cut down based on the most critical parts (where corrosion is maximum approximately). A very limited amount of fume was visible to the naked eye because of the cooling effect of continuous water. So, there was no disturbance when sharp blades came closer to it. After cutting the specimens were preserved in the laboratory at normal room temperature.

3.3 Cleaning bar specimens

Several cleaning techniques were reviewed for rust and residue removal:

- Acid Cleaning: Allows multiple bars to be cleaned at a time.
  - Cleaning time: 15-20 minutes
  - Yields dark brown finish after cleaning
- Sandblasting: Most commonly used method.

- Cleaning time: less than 15 minutes.
- Makes mat and granulated finish after cleaning.
- More visible pit than the other two methods (figure 11).

- Metallic brush: Not used in practical.
  - Cleaning time: Approximately 40 minutes to achieve the same cleaning capacity as mentioned above other two methods.
  - Gives a shiny smooth surface to corroded steel bars after application

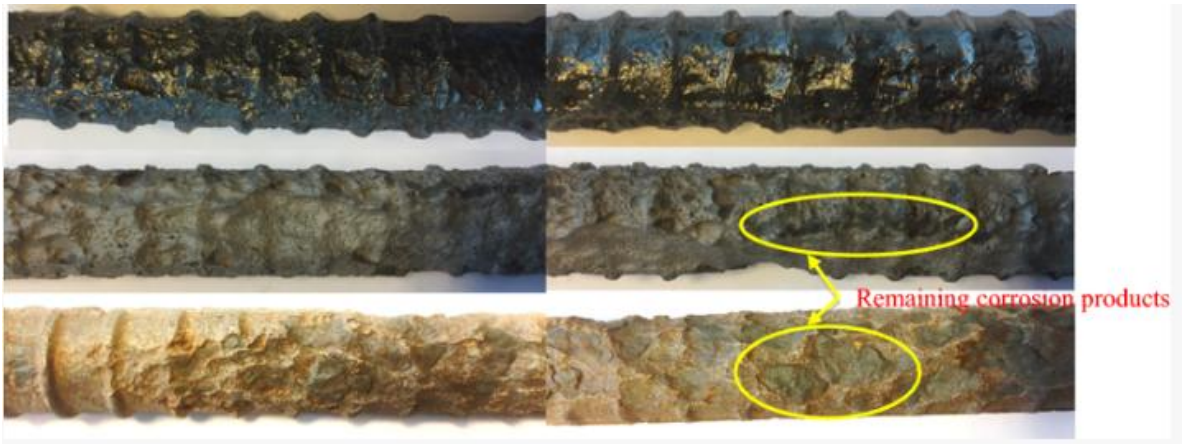

Figure 11: Surface cleaning process- metallic brushing, sandblasting & acid immersion (top to bottom)

Comparing the above three, abrasive sandblasting was chosen with silica sand as a medium for this particular research. Figure 12 shows sandblasted cabinet where the sand was blasted at 5-7 bars of pressure.

Figure 12: Sandblasting Cabinet

The sand used for the rust removal correlated to silica sand. The blast cabinet, a closed-loop system that lets the operator to blast the part and recycle the abrasive. It consists of these components: the cabinet, the abrasive blasting system, the abrasive recycling system,

and the dust collection. The operator treats the specimens from outside the cabinet by placing his arms into gloves attached to glove holes on the cabinet, later views it through a view window, and controls the blasting operation with a foot pedal. A pressure blast system was used and the sand abrasive was stored in the pressure vessel and sealed. The vessel was pressurized to match the pressure in the blast hose connected to its base. The abrasive was controlled as it entered the blast hose and then carried by the compressed air through the blast nozzle. Glass window was protected by a plastic sheet to avoid the diffusion of sand dust produced during blasting. It would leave the window clear almost even after abrasive and frequent blasting. A cylinder adjacent to the cabinet was used to place sand in the whole system. And hole attached to this allows fresh air through it and acted as a vacuum cleaner from the cabinet.

3.4 Determination of weight loss

- The gravimetric method was used to calculate the average corrosion degree based on weight loss before and after cleaning, using:

  Weight loss (%) = (Uncorroded Weight-Corroded Weight) *100/Uncorroded Weight

Table 4 below presents the computed weight-loss percentages for all specimens. This provided a reliable measure of average corrosion, which was later compared with localized corrosion determined from 3D scanning.

Specimen #	Specimen length(mm)	Weight of corroded rebars(g)	Weight of Un-corroded rebars(g)	Weight loss (%)
1	410	639.42	647.118	1.19
2	410	621.93	647.118	3.892
3	400	619.46	631.334	1.881
4	400	597.08	631.334	5.426
5	400	615.52	631.334	2.505
6	400	625.7	631.334	0.892
7	400	567.61	631.334	10.094
8	415	650.89	655.01	0.629
9	410	638.17	647.118	1.383
10	400	606.61	631.334	3.916
11	410	634.54	647.118	1.944
12	400	602.14	631.334	4.624
13	410	640.61	647.118	1.006
14	400	587.95	631.334	6.872
15	400	600.93	631.334	4.816
16	410	631.54	647.118	2.407
17	400	628.94	631.334	0.379
18	400	622.11	631.334	1.461
19	400	605.99	631.334	4.014
20	300	423.1	473.501	10.644
21	300	424.56	473.501	10.336
22	310	481.78	489.284	1.534
23	300	453.89	473.501	4.142
24	300	464.59	473.501	1.882
25	300	457.19	473.501	3.445
26	300	423.93	473.501	10.469
27	300	431.62	473.501	8.845
28	300	455.94	473.501	3.709
29	300	437.39	473.501	7.626
30	300	466.24	473.501	1.533
31	310	486.28	489.284	0.614
32	300	439.59	473.501	7.162
33	300	406.67	473.501	14.114
34	300	468.42	473.501	1.073
35	305	481.16	481.393	0.048
36	305	425.54	481.393	11.602
37	300	418.73	473.501	11.567
38	300	402.3	473.501	15.037
39	300	434	473.501	8.342

- 3D scanning techniques were employed to obtain a digital reconstruction of each specimen's outer surface (Table 4). The scanner enabled precise extraction of geometric parameters such as maximum diameter reduction, cross-sectional area loss and pit distribution along the bar. These digital models were later used for simulation-based corrosion quantification.

Although 3D scanning is widely applied in industrial and biomedical contexts, its use in civil engineering particularly for assessing reinforcement corrosion remains relatively novel. This study contributes to expanding its application in structural assessment.

Table 5, Average corrosion from computer simulations

Specimen #	Specimen length(mm)	Average corrosion (%)
1	410	1.650
2	410	5.040
3	400	10.0
4	400	12.610
5	400	6.090
6	400	6.560
7	400	9.565
8	415	4.070
9	410	5.894
10	400	7.670
11	410	4.257
12	400	17.866
13	410	5.100
14	400	9.344
15	400	9.468
16	410	5.785
17	400	5.591
18	400	9.369
19	400	15.500
20	300	17.505
21	300	6.312
22	310	6.666
23	300	8.560
24	300	6.496
25	300	8.247
26	300	15.466
27	300	6.758
28	300	7.856
29	300	10.931
30	300	12.220
31	310	7.345
32	300	10.268
33	300	17.930
34	300	6.858
35	305	5.747
36	305	5.672
37	300	13.318
38	300	11.583
39	300	13.897

3.5 Optical measurement techniques

Figure 13: Experimental setup showing the steel frame and 3D scanning device

The 3D scanning was performed using an industrial stereo optical system equipped with two 5-megapixel cameras providing 2 µm accuracy (Figure 13). Post-processing corrections such as mesh-hole filling, spike removal and surface smoothing were carried out using Geomagic Wrap 2014.

A Handy scan 3D device with 0.03 mm accuracy, 0.05 resolution and seven laser crosses was employed, integrated with VX Element software for acquisition. Two custom-built steel frames were used to hold the long (400 mm) and short (300 mm) specimens. The scanning process ensured nearly complete pit coverage and accurate geometry capture.

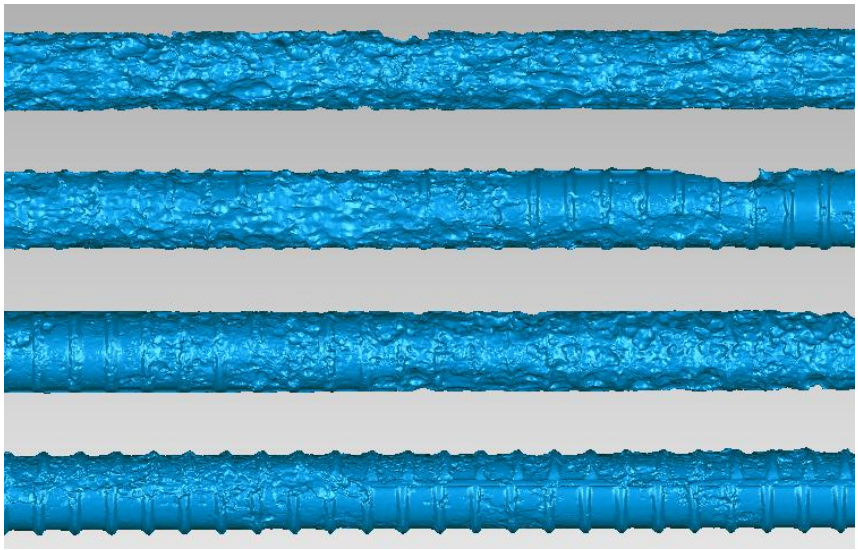

Figure 14: 3D surface model generated from VX element

Each scan produced a high-density triangular surface mesh of about 2-3 million elements (Figure 14 & 15), with an average element size of 0.014 mm^2. The global coordinate system (X, Y, Z) was defined from one bar end, allowing consistent reference across all specimens.

The level of detail enabled quantification of pit depth, length and cross-sectional loss along the rebar.

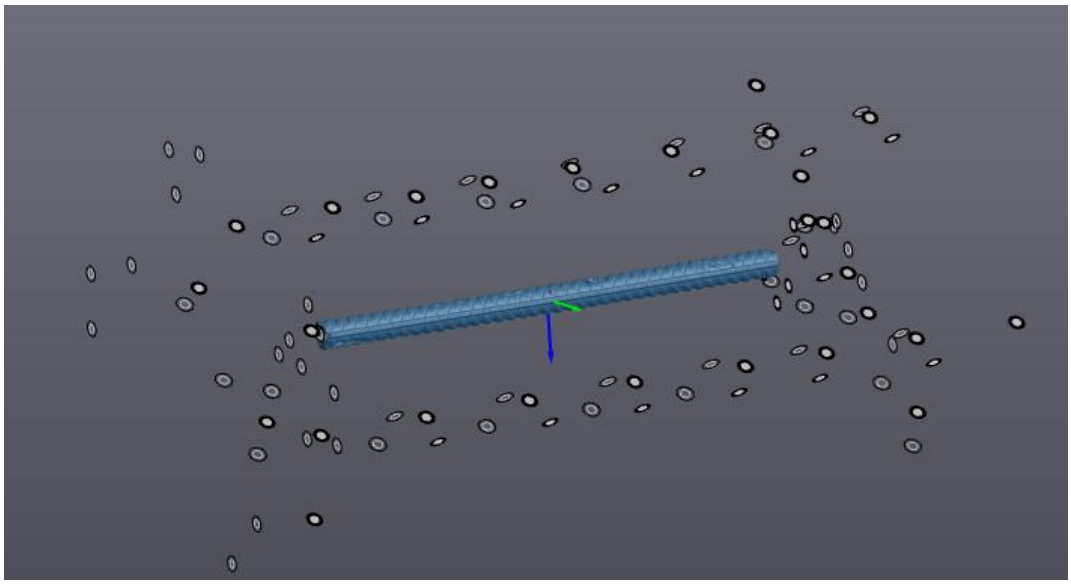

Figure 15: A general view of a corroded specimen with VX element scan results

Subsequently, files were exported as txt data and imported into Geomagic Wrap for refinement.

The main processing steps (Figures 16-17) included:

- Wrap: converting point clouds to polygon meshes.
- Mesh Doctor: repairing small holes, tunnels, spikes, tunnels and creases.
- Relax: smoothing mesh curvature.
- Fill All: closing holes from the bar polygon.
- Convert to points: reverting mesh surfaces to point clouds for further analysis.

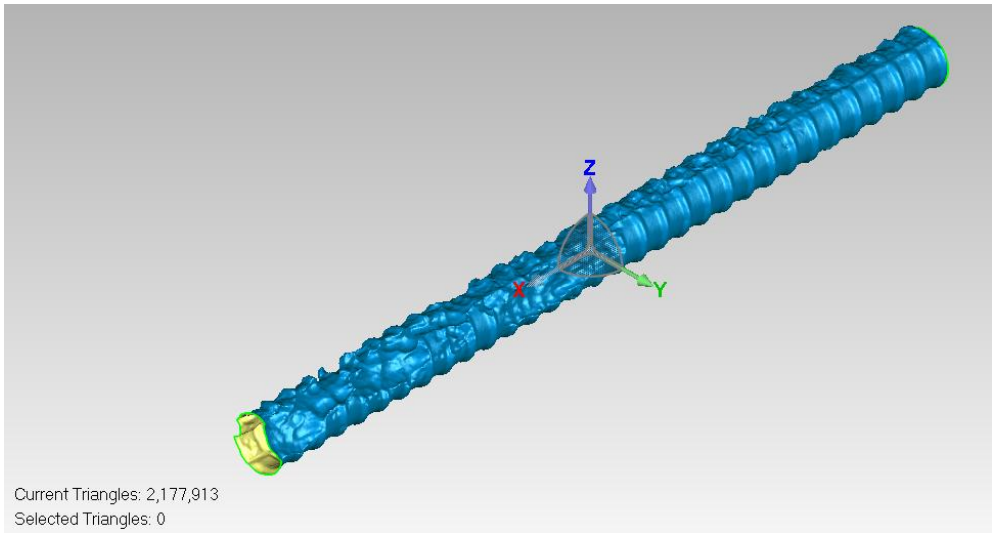

Figure 16: 3D Polygon mesh representation in Geomagic Wrap

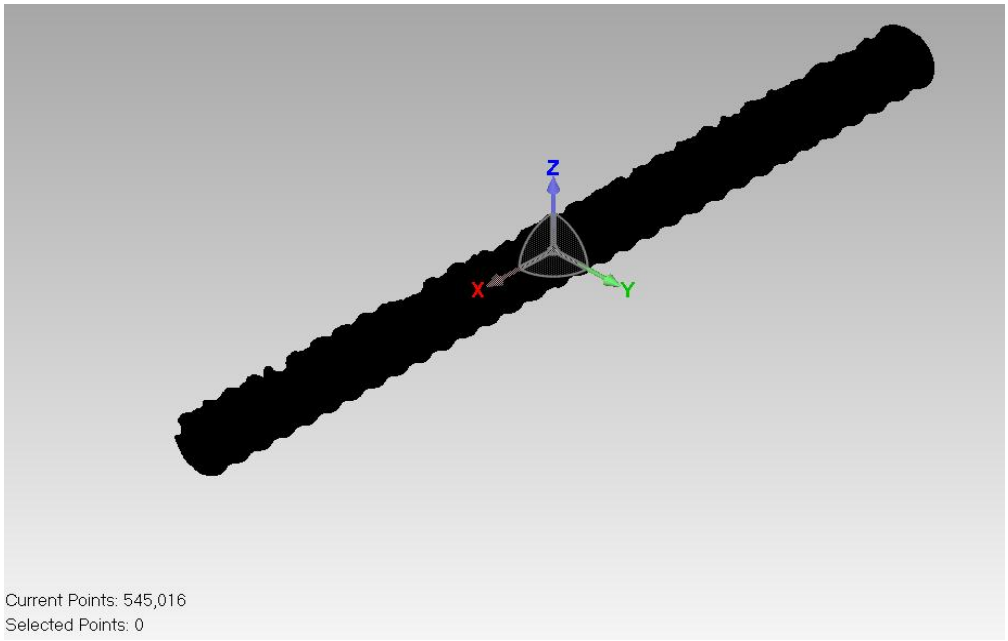

Figure 17: Conversion of polygon mesh into a point cloud in Geomagic Wrap

3.6 Summary

This chapter details the procedures for specimen preparation, cleaning, gravimetric corrosion assessment and 3D optical scanning. The combination of physical measurements and digital reconstruction provided complementary datasets, ensuring both macroscopic and microscopic insight into corrosion progression. The processed scan data were later used in MATLAB-based post-processing and simulations, described in Chapter 4, to analyze corrosion distribution and evaluate critical cross-sections.

4 Post-processing using MATLAB

4.1 Steps for simulation progress

The simulation of corrosion profiles was conducted using the ASC files obtained from Geomagic Wrap. The workflow proceeded as follows:

- Step 1: The ASC (ASCII) files, containing 3D point cloud data of the corroded specimens, were imported into MATLAB by dragging them into the workspace.
- Step 2: In the MATLAB import dialog, the following options were selected:
  - Data type: Numeric matrix
  - Delimiter: Space-separated values
- Step-3: The polygonal mesh exported from Geomagic Wrap had already been converted to point cloud data.
- Step-4: The imported matrix contained the three-dimensional coordinates (X, Y, Z) of the corroded bar surface. The data was limited to the scanned length of the bar, bounded by the start and end clipping planes defined during scanning.

4.2 Corrosion level evaluation

- First, the scanned geometry, figure 18a, was transformed into a cloud point mesh, preserving the measured surface shape.
- Second, the coordinates of each node (*X, Y, Z*), designated by the Cartesian coordinate system, were transformed into a polar coordinate system, which offered a more straightforward system for calculating the cross-sectional areas, defined by (θ, *r, x*), where θ was the angle with respect to cross-sectional *y-axis*, *r* the Euclidian distance of the point with concerning normal axis, and *x* the longitudinal coordinate *X* in global coordinates.
- Third, an interpolation of the current cloud data was performed into an explicitly user-supplied regular mesh grid defined by (θ', *x'*) that generate new interpolated *r'* values subordinated to each pair of (θ', *x'*) coordinates. Following this, the volumetrically corroded shape of the bar was represented as a 3D surface, where the y-axis shows the angle θ, x-axis follows the length of bar, and z- axis indicates the radius r. As a result of plotting this surface in a surface plot, it is possible to visualize the corrosion penetration along the bar surface, where the diverse colors directly relate to the corrosion penetration; see Figure 18b.
- Fourth, to determine the cross-sectional area at *x'*, the integration of the associate

  r' (θ', *x'*) was conducted as:

$$A(x') = \int_{-\pi}^{\pi} \frac{r'(\theta,x')^2}{2} \cdot d\theta' \qquad Eq$$

Subsequently, a function $A(x')$ was calculated and plotted as specified in blue in Figure 18c. As can be seen, this cross-sectional area varied along the bar due to the ribs. To eliminate the impact of the ribs on the cross-sectional changes along the bar, a cubic spline fit was performed, resulting in the red line in Figure 18c.

Moreover, an un-corroded zone of the bar was identified and its average cross-sectional area A_o was used as a reference. In the example shown in 18c, the un-corroded zone presents at the end of the bar, with the area (A_o) measuring 220 mm^2.

- Fifth, the smoothed cross-sectional area was normalized by A_o (figure 18d) which was later subtracted from 1(as full bar portion) to get corrosion percentages. In Figure 18e, the corrosion level obtained for one specific bar was clearly shown where the values varied from 0 to 33 %. In this way, average corrosion was found along bar length for each specific point location, the mean of all those values gave the average corrosion percentage for that particular bar specimen. By following this process average corrosion was found for all corroded specimen.

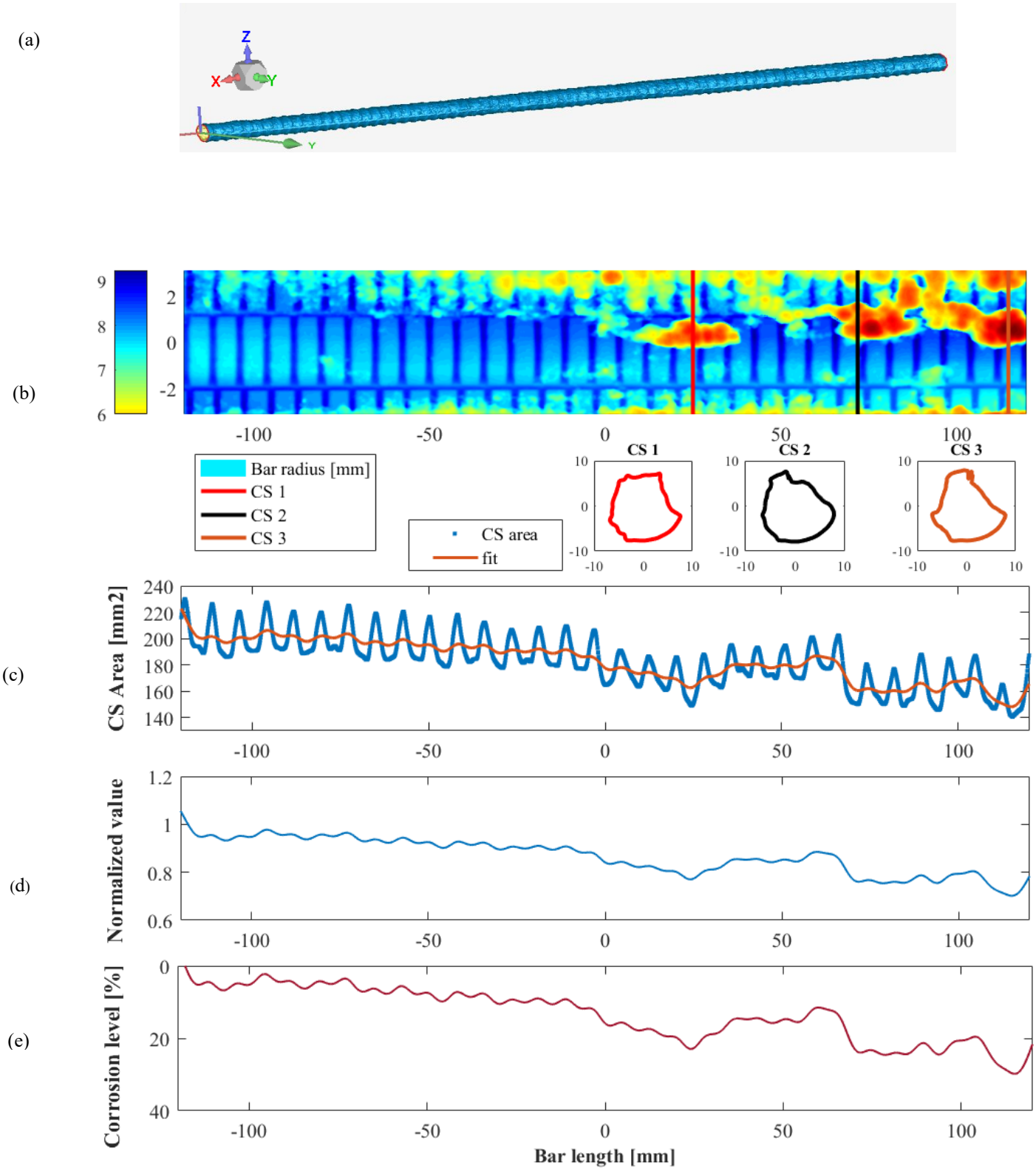

Figure 18: Overview of the method for determining corrosion percentage variations along a bar specimen

4.3 Simulation Outcome: Average Corrosion degree

The primary output from the simulation is the variation in cross-sectional area along each corroded bar, derived from 3D scanning data. This allows visualization and quantification of corrosion effects along the full length of the bar.

❖ **Visualization:**

In figure 19, the X-axis represents the longitudinal position along the bar in mm, while the Y-axis shows the corresponding retained cross-sectional area in mm^2 after corrosion.

Raw data points are plotted in blue, while a cubic spline best-fit curve (red) smooths local fluctuations, providing a continuous approximation of the residual cross-sectional profile.

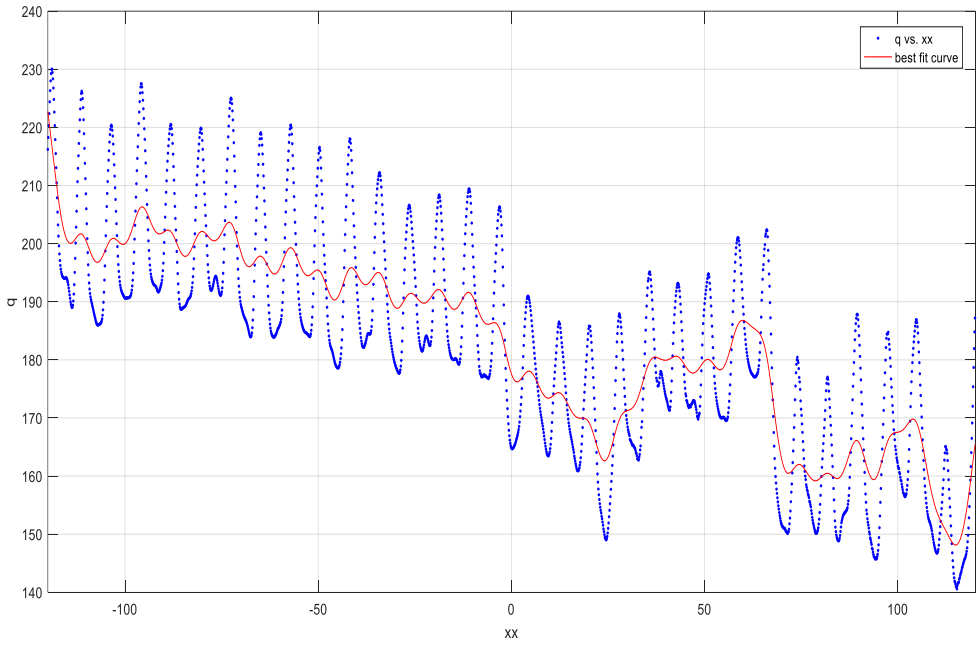

Figure 19: Cross-sectional area values(blue) and best-fit curve(red) plotted along the bar length (xx).

A clarified version of the best-fit line is presented separately in figure 20, showing smooth variation of the cross-section over the length of the specimen.

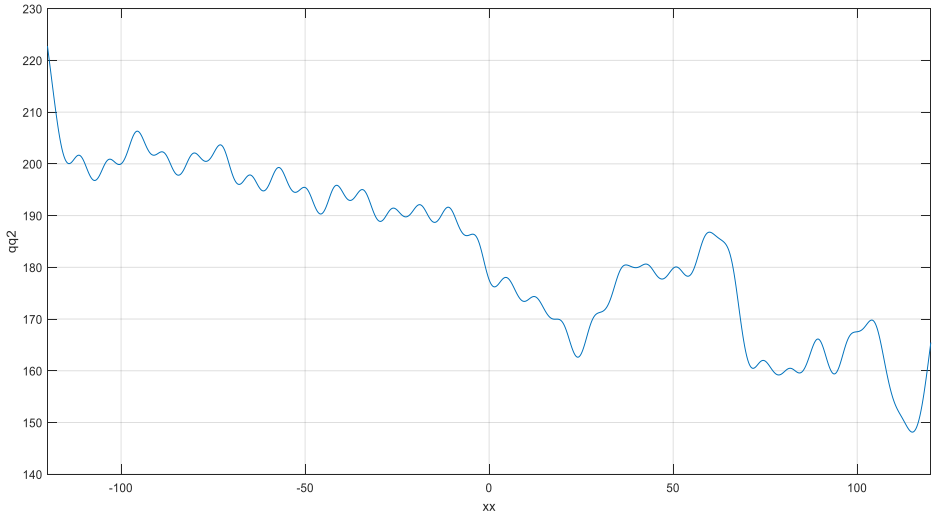

Figure 20: Best-fit cross-sectional areas (qq2) along the length of the steel bar specimen (xx)

❖ Normalization and Average Corrosion Calculation

In order to calculate the average corrosion degree, the best-fit cross-sectional values were normalized.

Normalized Area Fraction = $A_{retained}/A_0$

- $A_{retained}$ is the best-fit cross-sectional area at position x

- A_0 is the original cross-sectional area of an uncorroded bar

The mean of these normalized values along the full length of the bar represents the average uncorroded fraction of the bar's original section. To compute the average corrosion degree, this fraction was simply subtracted from 1.

Average Corrosion Degree = 1- Mean Normalized Area Fraction

Figure 21 illustrates the normalized cross-sectional area along the bar length for a typical specimen

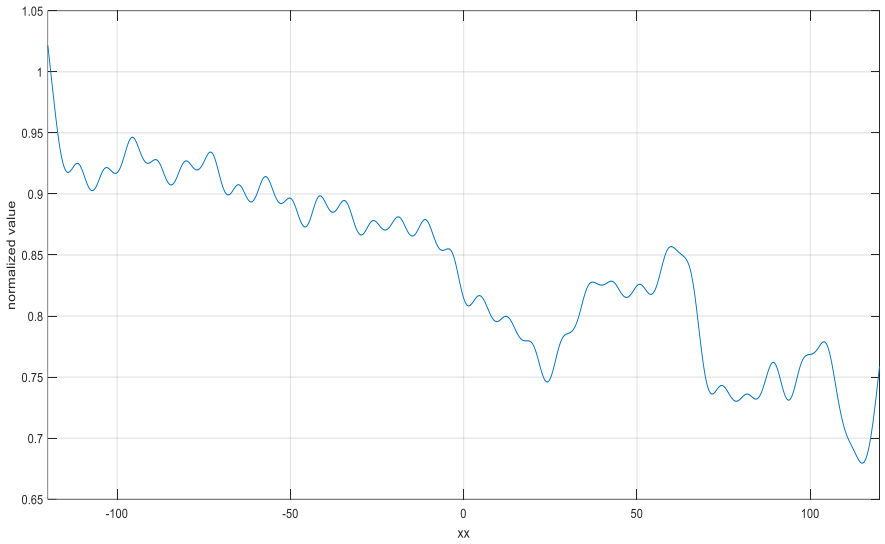

Figure 21: Normalized cross-sectional area values plotted along the bar length(xx)

5 Evaluation of Present Study

The present research focused on identifying and evaluating corrosion related parameters at the critical cross-sections of naturally corroded reinforcing bars. These parameters were obtained from high-resolution simulation data and are summarized in the following tables. Each value corresponds to the most severely deteriorated region (critical section) along the specimen length.

The objective of this evaluation was to explore relationships between localized corrosion indicators such as diameter reduction, cross-sectional area loss, perimeter variation and the average corrosion degree (%) derived from 3D simulations or the gravimetric method described in chapter 3.4.

Table 6 presents the main simulation outputs, including

- Corroded diameter at the most affected cross-section
- Critical cross-sectional area
- Critical perimeter
- Normalized ratios of these parameters relative to their uncorroded counterparts

Table 6: Specimen geometry and simulated critical corrosion parameters

Specimen #	bar length(mm) for simulation	Critical cross-sectional area, A_{crit} (mm^2)	Critical perimeter, P_{crit} (mm)	Uniform corroded diameter, d (mm)	d/d_0	P_{crit}/P_0	P_r/A_r
1	240	187.2	53.52	15.439	0.965	1.065	1.144
2	240	188.3	51.58	15.484	0.968	1.026	1.096
3	240	161.04	52.89	14.319	0.895	1.052	1.314
4	240	146.984	45.327	13.68	0.855	0.902	1.234
5	240	191.079	53.728	15.598	0.975	1.069	1.125
6	240	170.27	57.545	14.724	0.92	1.145	1.352
7	240	173.147	49.702	14.848	0.928	0.989	1.148
8	240	184.69	65.561	15.335	0.958	1.304	1.42
9	240	174.953	54.774	14.925	0.933	1.09	1.252
10	240	188.506	51.886	15.492	0.968	1.032	1.101
11	240	195.192	53.146	15.765	0.985	1.057	1.089
12	240	148.14	54.403	13.734	0.858	1.082	1.469
13	240	190.276	52.326	15.565	0.973	1.041	1.1
14	240	172.861	50.876	14.836	0.927	1.012	1.177
15	240	177.537	48.953	15.035	0.94	0.974	1.103
16	240	180.215	52.761	15.148	0.947	1.05	1.171
17	240	162.634	55.397	14.39	0.899	1.102	1.362
18	240	173.215	54.373	14.851	0.928	1.082	1.256
19	240	160.285	51.43	14.286	0.893	1.023	1.283
20	240	154.433	50.99	14.022	0.876	1.014	1.321
21	160	169.381	48.825	14.685	0.918	0.971	1.153
22	160	194.495	53.541	15.737	0.984	1.065	1.101
23	160	175.792	52.385	14.961	0.935	1.042	1.192
24	160	173.568	52.243	14.866	0.929	1.039	1.204
25	160	179.988	50.295	15.138	0.946	1.001	1.118
26	160	158.053	57.141	14.186	0.887	1.137	1.446
27	160	172.409	47.727	14.816	0.926	0.949	1.107
28	160	183.631	52.583	15.291	0.956	1.046	1.145
29	160	170.546	47.768	14.736	0.921	0.95	1.12
30	160	180.601	49.323	15.164	0.948	0.981	1.092
31	160	200.517	50.919	15.978	0.999	1.013	1.016
32	160	156.327	48.803	14.108	0.882	0.971	1.249
33	160	146.68	51.787	13.666	0.854	1.03	1.412
34	160	181.228	48.937	15.19	0.949	0.974	1.08
35	160	189.413	51.574	15.53	0.971	1.026	1.089
36	160	166.762	48.279	14.571	0.911	0.96	1.158
37	160	150.866	46.961	13.86	0.866	0.934	1.245
38	160	128.626	50.009	12.797	0.8	0.995	1.555
39	160	167.517	52.854	14.604	0.913	1.051	1.262

The pits observed in the corroded specimens were also measured manually using Vernier calipers. The pit geometry- length, width and depth was normalized with respect to the uncorroded bar diameter (d_0) to obtain dimensionless parameters, allowing for direct comparison between specimens of different sizes.

Meanwhile, simulations provided the maximum corrosion degree (%) at the critical cross-sections (CCS), the locations showing the most severe loss of material.

Table 7 summarizes both the average and maximum corrosion degrees obtained from the simulations, along with the pit geometry parameters (length, width and depth). The pit dimensions are also expressed as fractions of the uncorroded diameter (d_0), standardizing the degree of geometric degradation across all specimens.

Table 7: Average and maximum corrosion degree with normalized pit geometry parameters

Specimen #	Average corrosion degree from simulation (%)	Corrosion at CCS (%)	p_{length} (mm)	p_{width} (mm)	p_{depth} (mm)	p_{length}/d_0	p_{width}/d_0	p_{depth}/d_0
1	1.65	6.894	4.29	2.51	1.53	0.268	0.157	0.096
2	5.04	6.347	14.88	8.11	2.67	0.93	0.507	0.167
3	10	19.905	14.39	6.89	1.81	0.899	0.431	0.113
4	12.61	26.896	25.17	13.97	3.07	1.573	0.873	0.192
5	6.09	4.965	9.54	4.67	2.84	0.596	0.292	0.178
6	6.56	15.314	14.71	4.12	3.17	0.919	0.258	0.198
7	9.565	13.884	7.83	5.22	2.58	0.489	0.326	0.161
8	4.07	8.143	13.61	10	2.09	0.851	0.625	0.131
9	5.894	12.985	20.22	9.47	3.15	1.264	0.592	0.197
10	7.67	6.245	6.85	5.89	2.09	0.428	0.368	0.131
11	4.257	2.92	4.07	3.38	2.49	0.254	0.211	0.156
12	17.866	26.321	22.06	11.01	1.96	1.379	0.688	0.123
13	5.1	5.364	12.02	7.32	1.71	0.751	0.458	0.107
14	9.344	14.026	10.39	6.42	2.06	0.649	0.401	0.129
15	9.468	11.7	6.71	5.21	1.91	0.42	0.326	0.119
16	5.785	10.368	6.74	5.11	3.11	0.421	0.319	0.194
17	5.591	19.113	15.46	11.4	4.28	0.966	0.713	0.268
18	9.369	13.85	9.61	8.61	2.5	0.601	0.538	0.156
19	15.5	20.281	14.67	5.56	1.75	0.917	0.348	0.109
20	17.505	23.192	22.15	10.54	2.2	1.384	0.659	0.138
21	6.312	15.757	12.09	9.08	2.06	0.756	0.568	0.129
22	6.666	3.266	9.84	4.78	1.75	0.615	0.299	0.109
23	8.56	12.568	9.41	5.64	2.67	0.588	0.353	0.167
24	6.496	13.674	9.12	4.59	1.88	0.57	0.287	0.118
25	8.247	10.482	8.74	3.25	1.42	0.546	0.203	0.089
26	15.466	21.391	11.35	6.54	3.3	0.709	0.409	0.206
27	6.758	14.251	30.51	12.68	3.28	1.907	0.793	0.205
28	7.856	8.67	8.5	5.34	3.11	0.531	0.334	0.194
29	10.931	15.177	7.74	5.85	2.13	0.484	0.366	0.133
30	12.22	10.176	15.71	6.37	2.01	0.982	0.398	0.126
31	7.345	0.271	4.03	2.98	1.35	0.252	0.186	0.084
32	10.268	22.249	12.41	7.38	1.86	0.776	0.461	0.116
33	17.93	27.047	11.74	9.52	2.22	0.734	0.595	0.139
34	6.858	9.865	10.94	5.77	2.19	0.684	0.361	0.137
35	5.747	5.794	7.99	7.72	2.06	0.499	0.483	0.129
36	5.672	17.059	7.04	4.66	2.44	0.44	0.291	0.153
37	13.318	24.966	29.22	14.83	2.53	1.826	0.927	0.158
38	11.583	36.027	12.39	7.16	3.09	0.774	0.448	0.193
39	13.897	16.684	14.91	4.46	2.61	0.932	0.279	0.163

5.1 Results Summary in Classification Learner

To evaluate the relationship between critical corrosion parameters and average corrosion degree, the Classification Learner App in MATLAB was utilized. The response variable in this analysis was the average corrosion degree of the corroded steel specimens. Since this average corrosion degree was obtained using two different methods, the gravimetric (weight-loss) method and the 3D simulation- based estimation, the objective was to identify which data-set better correlates with the maximum corroded parameters observed at critical cross-sections.

The Classification Learner was used to test multiple predictor-response combinations and classifier types. The highest-performing models, along with their corresponding accuracy percentages, are summarized in Table 8 and Table 9. Each predictor variable represents a geometric or physical feature associated with the most critically corroded cross-sections.

Table 8: Classification Results (Gravimetric average corrosion as Response)

Features	Response	Predictor	Best Model	Classifier	Accuracy
1	average corrosion degree (wt. loss)	p_{width}	Fine, Medium, Coarse Gaussian	SVM	12,80%
2		p_{depth}	Coarse Gaussian	SVM	12,80%
3		Corrosion at CCS	Coarse Gaussian	SVM	12,80%
4		d/d_0	Coarse Gaussian	SVM	12,80%
5		p_{depth}/d_0	Coarse Gaussian	SVM	12,80%
6		p_{width}/d_0	Coarse Gaussian	SVM	12,80%
7		p_{length}/d_0	Coarse Gaussian	SVM	12,80%
8		P_{crit}/P_0	Coarse Gaussian	SVM	7,7%
9		P_r/A_r	Coarse Gaussian	SVM	12,80%

Table 9: Classification Results (Simulation based average Corrosion as Response)

Features	Response	Predictor	Best Model	Classifier	Accuracy
1	average corrosion degree (simulation)	p_{width}	Fine, Medium, Coarse Gaussian	SVM	12,80%
2		p_{depth}	Coarse Gaussian	SVM	12,80%
3		Corrosion at CCS	Coarse Gaussian	SVM	12,80%
4		d/d_0	Coarse Gaussian	SVM	12,80%
5		p_{depth}/d_0	Coarse Gaussian	SVM	12,80%
6		p_{width}/d_0	Coarse Gaussian	SVM	12,80%
7		p_{length}/d_0	Coarse Gaussian	SVM	12,80%
8		P_{crit}/P_0	Coarse Gaussian	SVM	10,30%
9		P_r/A_r	Coarse Gaussian	SVM	12,80%

Key Observations:

- Across both datasets, the highest classification accuracy (~12.80%) was consistently achieved using Support Vector Machine (SVM) models with Gaussian kernels of varying widths (fine, medium, coarse).

- The only notable exception was Feature 8 (P_{crit}/P_0), where the simulation-based data performed slightly better (10.30%) than the gravimetric-based data (7.70%). This suggests that simulation- derived parameters may provide more reliable input for predictive modeling.

- Pit depth was manually measured following the same approach as other geometric parameters. However, multiple pits might exist within a single cross-section, and these were not accounted for potentially introducing measurement error. A more precise instrument, such as a laser profilometer would improve accuracy.

- Despite experimenting with multiple Gaussian SVM models, overall classification accuracy remained low which indicates that the relationship between the selected features and corrosion levels is likely weak, nonlinear or data-limited.

5.2 Discussion of findings

The consistently low classification accuracy across both data sets reflects the inherent difficulty of establishing a reliable relationship between average and maximum corrosion at critical steel sections. Corrosion in steel reinforcement is naturally non-uniform, influenced by local concrete properties, environmental exposure and microstructural variations. As a result, simple classification approaches struggle to represent the complex, non- linear relationships inherent in the data, particularly when relying on a limited number of manually obtained features.

Although the machine learning models did not produce high predictive accuracy, the analysis still yields important insights that connect directly to the research gaps identified in the literature:

1. Simulation-based data are more reliable than manual measurements. The simulation-based results performed slightly better, showing that high-resolution digital scanning gives more consistent and accurate measurements than manual or weight loss methods.

2. Critical geometric features are weakly related to average corrosion. Features like pit width, depth and cross-sectional ratios did not predict maximum corrosion well. This suggests that other factors, such as pit density or micro structure, may also be important.

3. Classification may not be the best approach. Since corrosion progression is continuous and nonlinear, regression or correlation analysis could better show the relationship between average and maximum corrosion. Machine learning can help, but it needs larger and more detailed datasets to work well.

4. Even low accuracy gives useful information. The results show the limits of current methods and point to improvements for future studies, such as using higher-resolution scanning, more samples, or combining manual, gravimetric and digital data.

Overall, the study shows that predicting extreme corrosion from average values is challenging. However, it confirms that 3D scanning and simulation data are useful for understanding corrosion patterns and can help engineers estimate the worst-case damage more reliably.

6 Response-Predictor Relations

The current analysis investigates the relationships between average corrosion degree (used as the sole response variable) and various geometric predictors at critical corroded sections. The goal is to identify whether strong or consistent trends exist between average corrosion and local parameters such as pit width, pit depth, diameter reduction, or perimeter loss. Each parameter was plotted against the average corrosion degree to identify trends and test their suitability for predictive modeling. The following figures provide a visual representation of these response–predictor relations, along with observations drawn from both manual and simulation-based data.

Pit Width: An increasing trend is observed between pit width and average corrosion degree, indicating that wider pits are generally associated with more severe corrosion. However, the data points show considerable scatter, reflecting variability from manual measurements and irregular pit geometries (Figure 22).

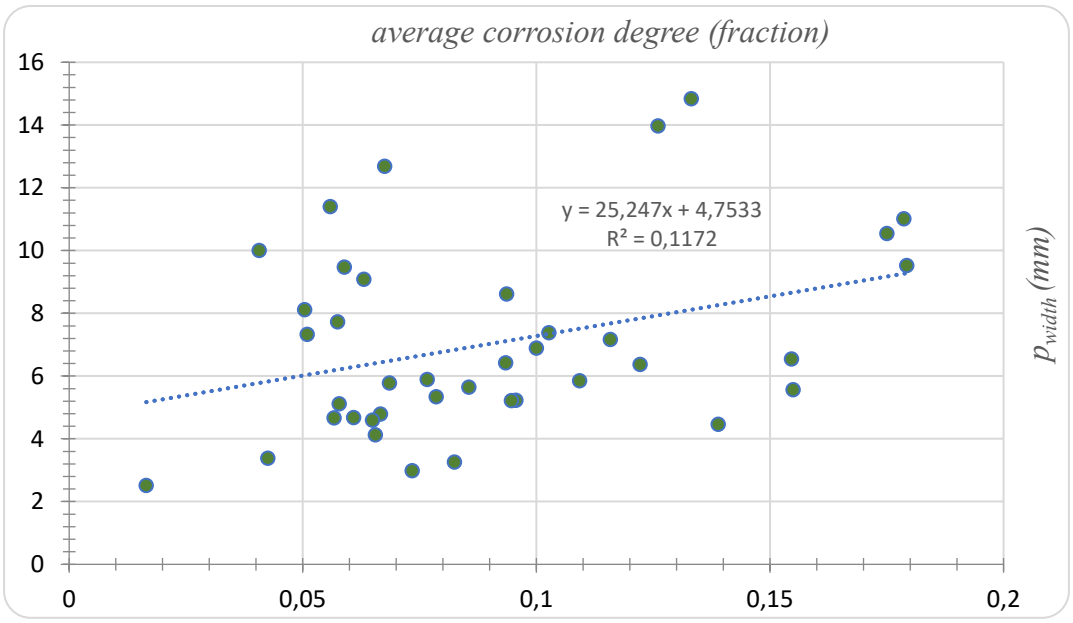

Figure 22: Pit width in relation to average corrosion degree

Pit Depth: Pit depth exhibits a relatively flat or inconsistent trend against average corrosion degree, suggesting no strong correlation. This may be due to the complex morphology of pits and limitations in manual measurement accuracy (Figure 23).

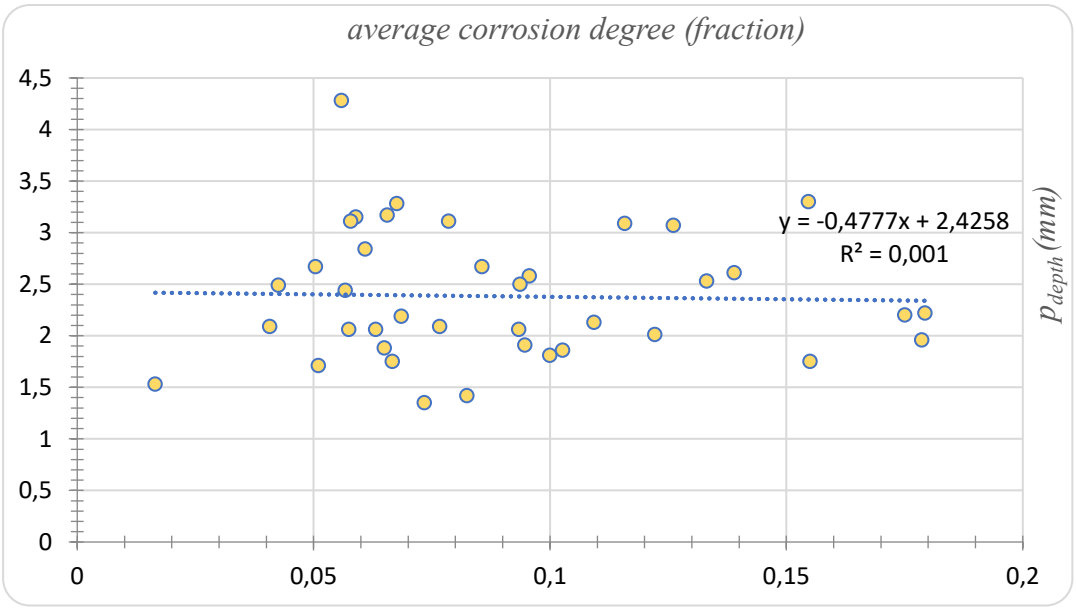

Figure 23: Pit depth compared with average corrosion degree

Corrosion at Critical Cross-Section (CCS): A positive trend is visible, where higher average corrosion levels align with increased corrosion at the critical section. The closer fit of data points to the trend line indicates a potentially meaningful relationship, despite minor deviations (Figure 24).

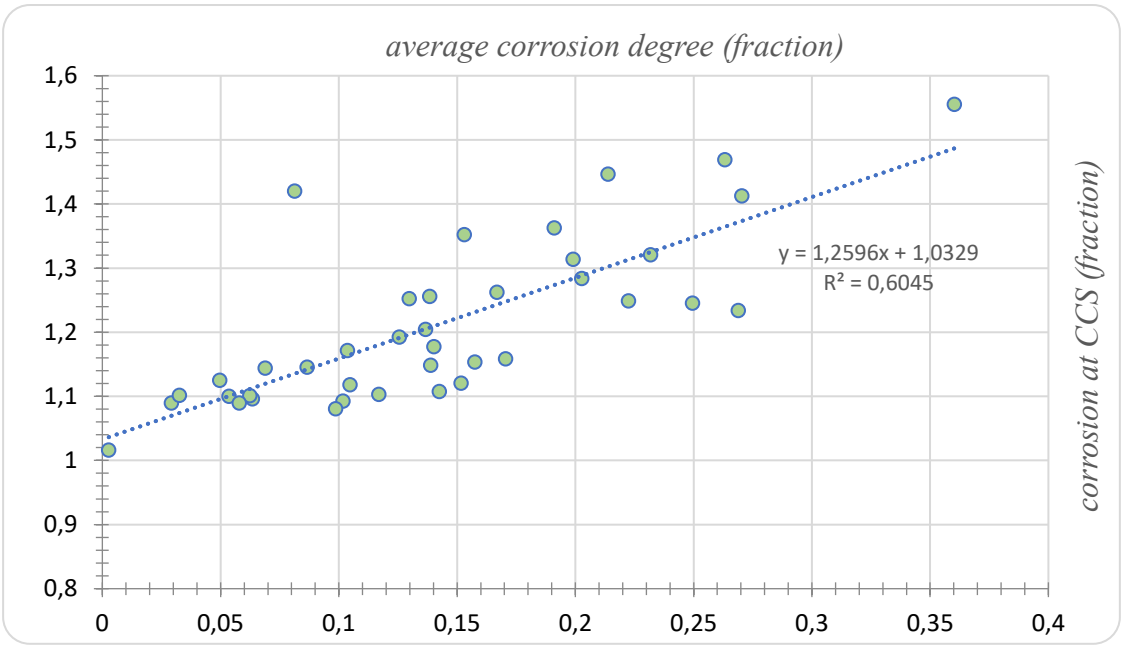

Figure 24: Corrosion level at the critical cross-section (CCS) for varying average corrosion

Diameter Reduction (d/d_0): A clear decreasing trend is observed, showing that higher average corrosion corresponds to greater reductions in bar diameter. This ratio serves as a useful geometric indicator of corrosion severity (Figure 25).

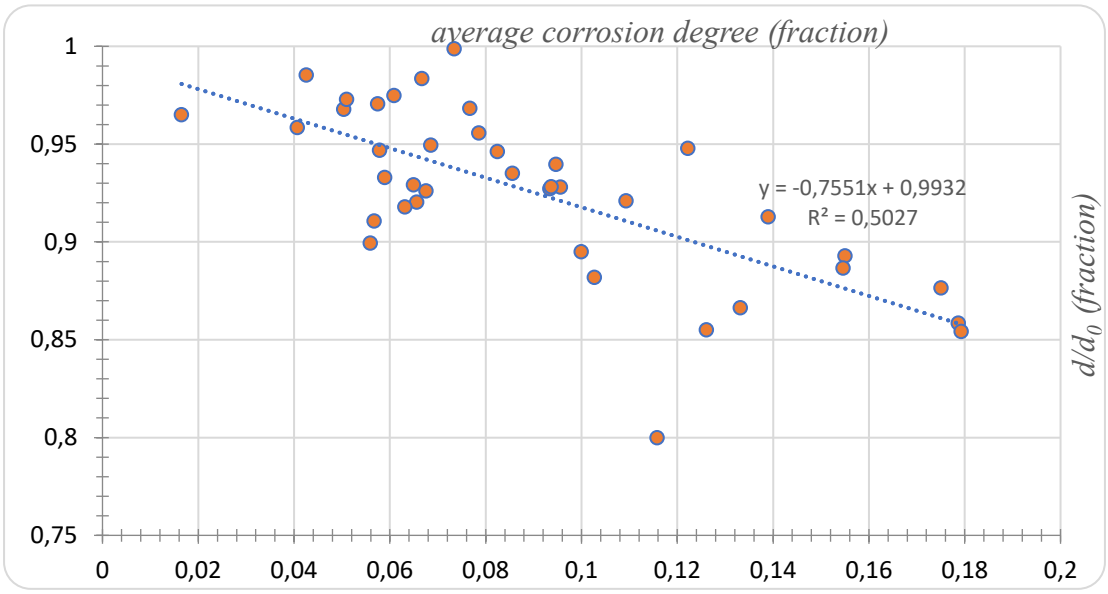

Figure 25: Diameter reduction ratio (d/d_0) with increasing average corrosion

Normalized Pit Depth (p_{depth}/d_0): The correlation with average corrosion is weak, with significant scatter, indicating that normalized pit depth may not reliably scale with overall corrosion due to local variability (figure 26).

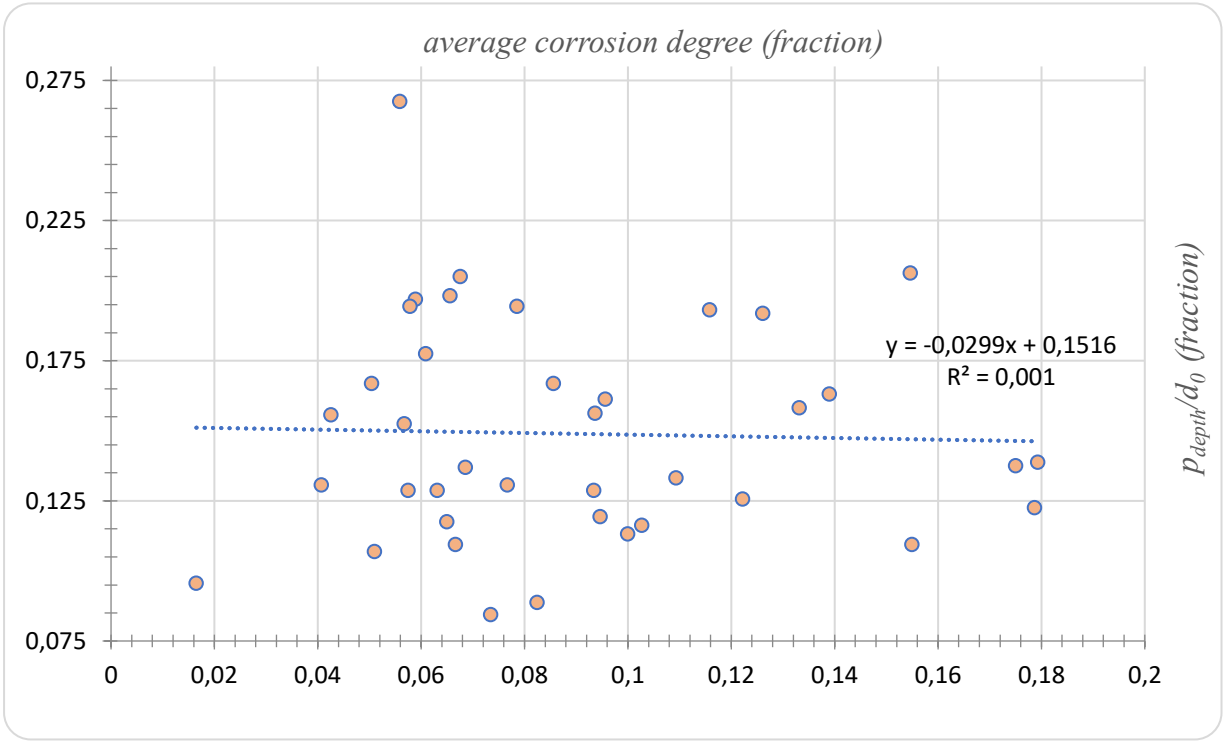

Figure 26: Normalized pit depth (p_{depth}/d_0) across corrosion levels

Normalized Pit Width (p_{width}/d_0): Pit width normalized by original bar diameter shows a rising trend with increasing average corrosion, though not strictly linear. This suggests that

pit expansion is partly influenced by overall mass loss but also by localized corrosion behaviour (Figure 27).

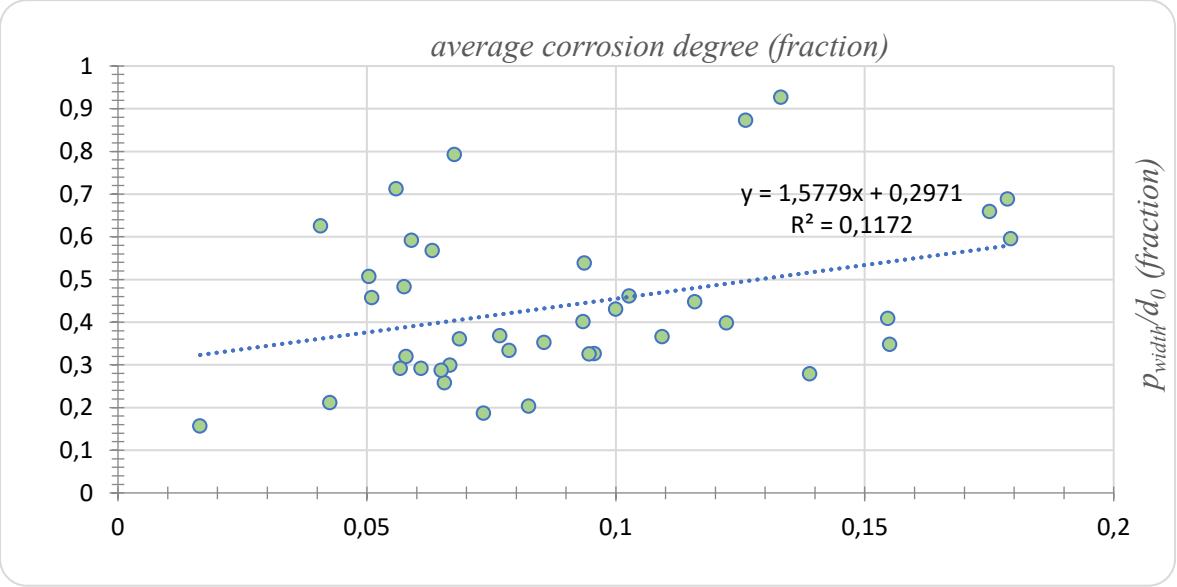

Figure 27: Normalized pit width (p_{width}/d_0) as corrosion progresses

Normalized Pit Length (p_{length}/d_0): Similar to normalized pit width, pit length shows scattered correlation with average corrosion, reflecting irregular pit growth patterns along the bar surface (Figure 28).

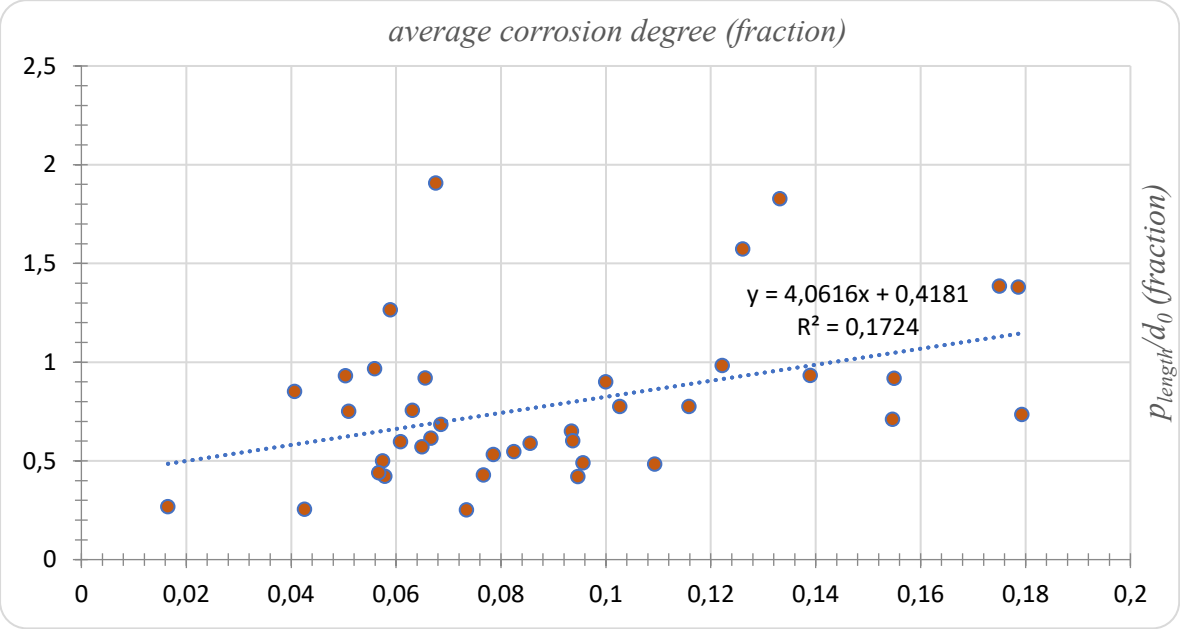

Figure 28: Normalized pit length (p_{length}/d_0) versus corrosion degree

Normalized Critical Perimeter (P_{crit}/P_o): A declining trend is observed, showing that corrosion progressively reduces the perimeter at the most affected section of the bar. The nonlinear pattern indicates that, at early corrosion stages, the perimeter decreases gradually. However, after a certain corrosion level, the reduction becomes more rapid. This acceleration occurs due to the combined effects of localized pitting, irregular section loss and deep corrosion penetration, which significantly reduces effective perimeter of the bar (Figure 29).

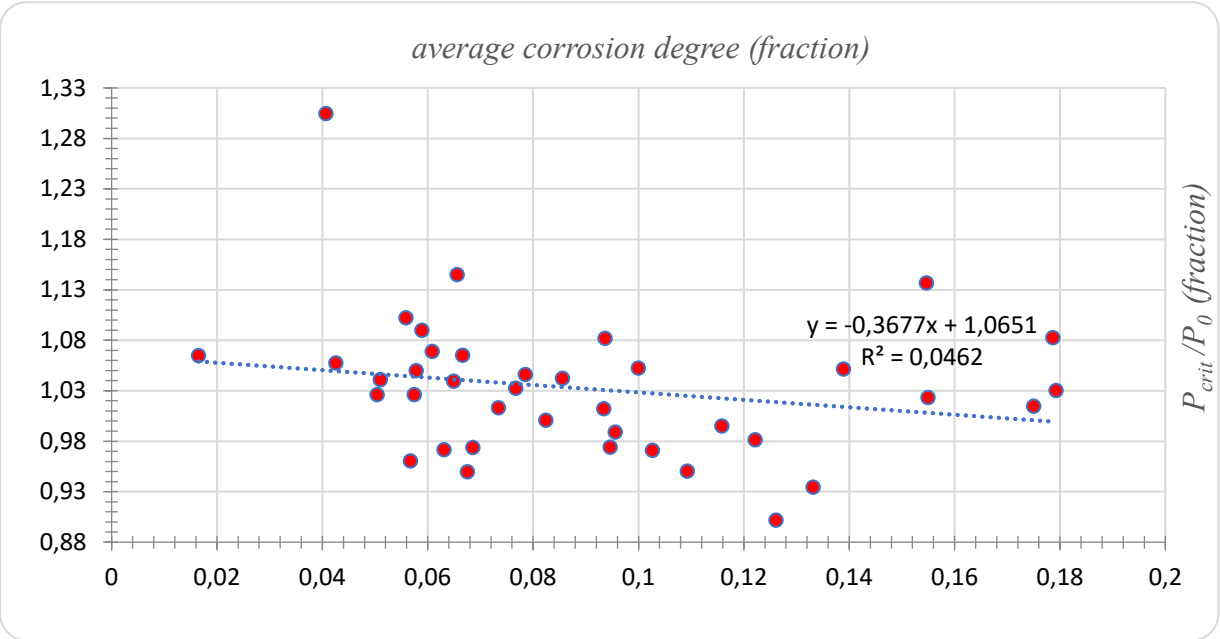

Figure 29: Reduction of normalized critical perimeter (P_{crit}/P_0) due to corrosion progression

Perimeter to Area Ratio (P_r/A_r): This ratio increases with average corrosion, showing that cross-sectional area degrades more severely than perimeter. This indicates a shift toward more localized, intense pitting at higher corrosion levels (Figure 30).

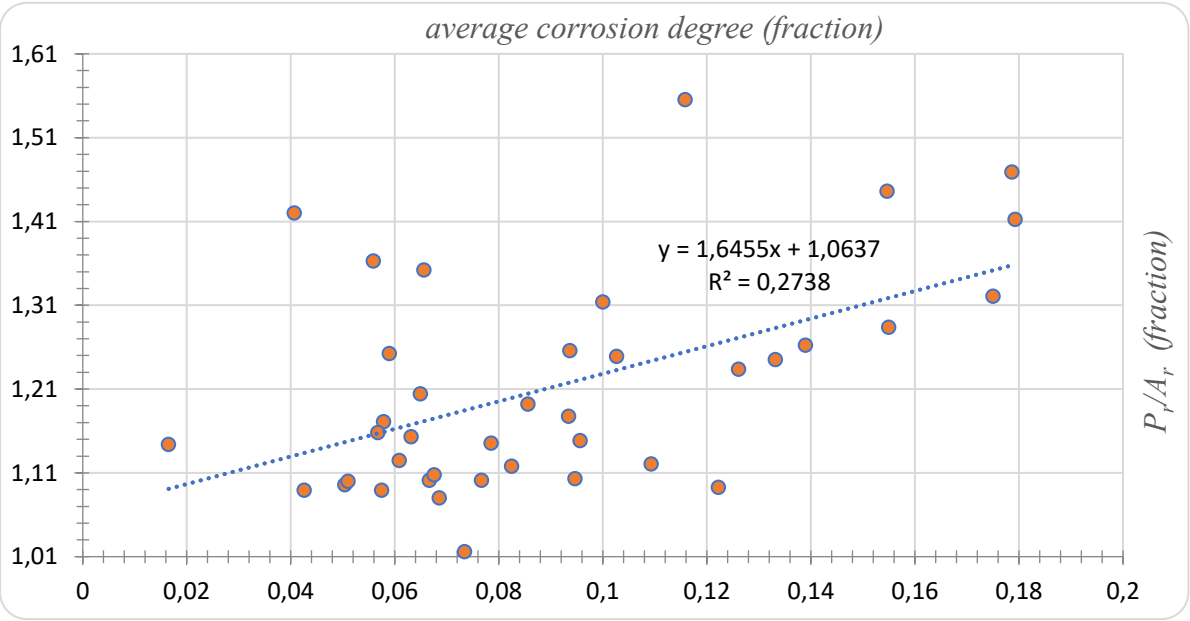

Figure 30: Ratio of perimeter reduction to area reduction (P_r/A_r) across corrosion levels

7 Conclusion

This research was structured as a comprehensive scheme combining experimental work, computer simulations, and manual data processing to investigate corrosion behaviour in naturally degraded steel reinforcing bars. A total of thirty-nine corroded specimens were analyzed to determine their average corrosion degree and to identify their most deteriorated (critical) cross-sections. Various geometric and corrosion-related parameters were evaluated at these critical locations to investigate their relationship with the average corrosion degree.

The process began with the mechanical preparation of the steel bars, including cutting and sandblasting to remove corrosion products. Thereafter, 3D scanning was conducted to obtain high-resolution surface profiles of the specimens. These scans were processed using MATLAB-based simulations to extract detailed geometric parameters and corrosion metrics.

Based on previous discussions, the following conclusions can be drawn:

1. **Discrepancy in average corrosion measurement methods**:

The average corrosion degrees obtained through gravimetric and simulation methods did not match exactly. Gravimetric analysis included the mass of corrosion products, resulting in slightly lower corrosion estimates. In contrast, simulations captured the geometry of cleaned pits only, thereby reflecting higher and likely more accurate corrosion degrees. Ideally, weighing after cleaning would have aligned the results more closely, but this was not feasible due to time constraints and lab availability.

2. **Independence from bar size:**

Predictor variables such as normalized pit width (p_{width}/d_0), pit depth (p_{depth}/d_0) and perimeter ratios were independent of bar diameter or length, conforming that these parameters can describe corrosion behaviour irrespective of specimen dimensions.

3. **Behaviour of geometric predictors**:

   – Pit width increased with corrosion degree, though data scatter indicated irregular surface attack.

   – Pit depth showed inconsistent correlation, suggesting that deeper pits can occur even when the total corrosion of the bar is relatively low.

   – The ratio (d/d_0) decreased steadily, evidencing uniform cross-sectional reduction.

   – Normalized pit dimensions (p_{width}/d_0, p_{length}/d_0) displayed moderate to weak trends, implying variability in local morphology.

   – As corrosion progresses, P_{crit}/P_0 declined non-linearly while P_r/A_r raised, revealing progressive section deterioration with intensified localized pitting.

4. **Interpretation of corrosion morphology**:

At lower corrosion levels, the steel bars exhibited broadly uniform surface degradation, with consistent diameter and area loss. As corrosion advanced, evidence of localized

intensification appeared, particularly reflected in the rising P_r/A_r ratio and scattered pit geometry indicating a transition toward mixed corrosion behaviour.

5. **Predominant corrosion type**:

Overall, the corrosion pattern can be described as mainly uniform, governing the general mass loss, yet evolving into localized pitting at critical sections. This mixed pattern reflects the natural transition from surface-level corrosion to deeper localized attack as exposure conditions and anodic-cathodic activity become uneven along the bar.

6. **Limitations and future scope**:

Some uncertainty persists in manual data due to limited resolution and model prediction accuracy. Future studies should include tensile or pull-out testing to link geometric degradation with actual mechanical implications, thereby providing a more complete understanding of corrosion impact on reinforcement performance.

References

1. Apostolopoulos, C.A. (2007). Mechanical behaviour of corroded reinforcing steel bars S500s tempcore under low cycle fatigue. Construction and Building Materials, 21(7), 1447-1456. https://doi.org/10.1016/j.conbuildmat.2006.07.008

2. Bains, M.S., Singh, Y., Singh, H. (2024). Flexural response of corroded RC members: A review. International Research Journal of Engineering and Technology (IRJET), 11(8), 841-849. Retrieved from https://www.irjet.net/archives/V11/i8/IRJET-V11I841.pdf

3. Bamforth, P.B., 2002. Concrete Durability by Design: Limitations of the current prescriptive approach and alternative methods for durability design. Building Research Establishment, Crowthorne, UK. Retrieved from https://cdn.ymaws.com/concretenz.org.nz/resource/resmgr/docs/conf/2002/s1_keynote_-_bamforth.pdf

4. Chen, Y., & Zhou, Y. (2025). Study on the corrosion patterns of rebar in concrete based on CT detection technology. Construction and Building Materials, 467, 140333 https://doi.org/10.1016/j.conbuildmat.2025.140333

5. Fernández, I., Bairán, J. M., & Marí, A. R. (2015). Corrosion effects on the mechanical properties of reinforcing steel bars: fatigue and σ–ε behavior. *Construction & Building Materials, 101*, 722–783. https://doi.org/10.1016/j.conbuildmat.2015.10.139

6. Fernandez, I., Bairán, J. M., Marí, A. R. (2016). 3D FEM model development from 3D optical measurement technique applied to corroded steel bars. Construction and Building Materials, 124, 519-532.https://doi.org/10.1016/j.conbuildmat.2016.08.020

7. Fernández, I., Bairán, J. M., & Marí, A. R. (2016). Mechanical model to evaluate steel reinforcement corrosion effects on σ–ε and fatigue curves: experimental calibration and validation. Engineering Structures, 118, 320–333. https://doi.org/10.1016/j.engstruct.2016.03.055

8. Fernández, I., & Berrocal, C. G. (2019). Mechanical Properties of 30-Year-Old Naturally Corroded Steel Reinforcing Bars. International Journal of Concrete Structures and Materials, Volume 13, Article 9. https://doi.org/10.1186/s40069-018-0308-x

9. Fernandez, I., Lundgren, K., Zandi, K. (2018). Evaluation of corrosion level of naturally corroded bars using different cleaning methods, computed tomography, and 3D optical scanning. Materials and Structures, 51, 78. https://doi.org/10.1617/s11527-018-1206-z

10. Iannuzzi, M., Hornus, E., Salasi, M. (2022). Chapter 2: Crevice corrosion. In ASTM International eBooks. https://doi.org/10.1520/mnl202ndsup20190034

11. Istrate, G.G., Negru, I., Babencu, D.-F. (2023). Evaluation of corrosion behaviour by gravimetric method. The Annals of "Dunarea de Jos" University of Galati, Fascicle IX. Metallurgy and Materials Science, 46(4), 37-41. https://doi.org/10.35219/mms.2023.4.06

12. Nanan, K. (2019). Understanding pitting corrosion to prevent catastrophic failures. Retrieved from https://www.corrosionpedia.com/all-about-pitting-corrosion/2/6590

13. Reichenbach, S., Preinstorfer, P., Hammerl,M., Kromoser, B. (2021). A review on embedded fibre-reinforced polymer reinforcement in structural concrete in Europe. Construction and Building Materials, 30,124946.https://doi.org/10.1016/j.conbuildmat.2021.124946

14. Rizhang, Z., Guo, J., Xu, K. (2023). Intergranular corrosion: The ECPH Encyclopedia of Mining and Metallurgy.https://doi.org/10.1007/978-981-19-0740-1_435-1

15. Wang, H.L., Sun, X.Y., Kong H.T. (2018). Effect of corrosion and corrosion rate on the mechanical performance of carbon and stainless-steel reinforcing bars. In Proceedings of the Sixth International Conference on Durability of Concrete Structures (Paper PSE09, pp. 390-394). University of Leeds, Leeds, UK. https://docs.lib.purdue.edu/cgi/viewcontent.cgi?article=1212&context=icdcs

16. Xiong, Y., Wu, D., Tang, Y., Shu, H. (2017). Experimental studies on mechanical properties of corroded steel bars after elevated temperature. Procedia Engineering, 210, 622-629. https://doi.org/10.1016/j.proeng.2017.11.122

17. Xu, Y. (2015). The corrosion characteristics and tensile behaviour of reinforcement under coupled carbonation and static loading. Materials, 8(12), 8561-8577. https://doi.org/10.3390/ma8125479

18. Yan X., Di, W., Yingfeng, T., Minque, H., Hai, S. (2017). Experimental studies on mechanical properties of corroded steel bars after elevated temperature. Procedia Engineering, 210, 622-629. https://doi.org/10.1016/j.proeng.2017.11.122

19. Zeng, S., Gu, S., Ren, S., Gu, Y., Kong, C., Yang, L. (2022). A Modeling method for Finite Element Analysis of Corroded Steel Structures with Random Pitting Damage. Buildings, 12(11), 1793. https://doi.org/10.3390/buildings12111793

20. Zhang, W., Song, X., Gu, X., Li, S. (2012). Tensile and fatigue behaviour of corroded rebars. Construction and Building Materials, 34, 409-417. https://doi.org/10.1016/j.conbuildmat.2012.02.071

Appendix A- MATLAB Script for Corrosion Simulation from Bar (1-39)

```
vv=F(N,T);
yl=[-3.1416;3.1416];
xl=[xx(692);xx(692)];
xl2=[xx(850);xx(850)];
xl3=[xx(1317);xx(1317)];
[yc.a,zc.a]=pol2cart(tu,vv(:,692));
[yc.b,zc.b]=pol2cart(tu,vv(:,850));
[yc.c,zc.c]=pol2cart(tu,vv(:,1317));
%set here the average uncorroded area
avga= 210;
% Calculate perimeter of each section
```

```
vv=F(N,T);
yl=[-3.1416;3.1416];
xl=[xx(375);xx(375)];
xl2=[xx(525);xx(525)];
xl3=[xx(1326);xx(1326)];
[yc.a,zc.a]=pol2cart(tu,vv(:,375));
[yc.b,zc.b]=pol2cart(tu,vv(:,525));
[yc.c,zc.c]=pol2cart(tu,vv(:,1326));
%set here the average uncorroded area
avga= 210;
% Calculate perimeter of each section
```

```
vv=F(N,T);
yl=[-3.1416;3.1416];
xl=[xx(257);xx(257)];
xl2=[xx(380);xx(380)];
xl3=[xx(709);xx(709)];
[yc.a,zc.a]=pol2cart(tu,vv(:,257));
[yc.b,zc.b]=pol2cart(tu,vv(:,380));
[yc.c,zc.c]=pol2cart(tu,vv(:,709));
%set here the average uncorroded area
avga= 213.5532;
% Calculate perimeter of each section
```

```
vv=F(N,T);
yl=[-3.1416;3.1416];
xl=[xx(790);xx(790)];
xl2=[xx(1209);xx(1209)];
xl3=[xx(1542);xx(1542)];
[yc.a,zc.a]=pol2cart(tu,vv(:,790));
[yc.b,zc.b]=pol2cart(tu,vv(:,1209));
[yc.c,zc.c]=pol2cart(tu,vv(:,1542));
```

```
vv=F(N,T);
yl=[-3.1416;3.1416];
xl=[xx(58);xx(58)];
xl2=[xx(337);xx(337)];
xl3=[xx(1130);xx(1130)];
[yc.a,zc.a]=pol2cart(tu,vv(:,58));
[yc.b,zc.b]=pol2cart(tu,vv(:,337));
[yc.c,zc.c]=pol2cart(tu,vv(:,1130));


vv=F(N,T);
yl=[-3.1416;3.1416];
xl=[xx(58);xx(58)];
xl2=[xx(503);xx(503)];
xl3=[xx(674);xx(674)];
[yc.a,zc.a]=pol2cart(tu,vv(:,58));
[yc.b,zc.b]=pol2cart(tu,vv(:,503));
[yc.c,zc.c]=pol2cart(tu,vv(:,674));


vv=F(N,T);
yl=[-3.1416;3.1416];
xl=[xx(1);xx(1)];
xl2=[xx(292);xx(292)];
xl3=[xx(350);xx(350)];
[yc.a,zc.a]=pol2cart(tu,vv(:,1));
[yc.b,zc.b]=pol2cart(tu,vv(:,292));
[yc.c,zc.c]=pol2cart(tu,vv(:,350));


vv=F(N,T);
yl=[-3.1416;3.1416];
xl=[xx(833);xx(833)];
xl2=[xx(1001);xx(1001)];
xl3=[xx(1401);xx(1401)];
[yc.a,zc.a]=pol2cart(tu,vv(:,833));
[yc.b,zc.b]=pol2cart(tu,vv(:,1001));
[yc.c,zc.c]=pol2cart(tu,vv(:,1401));

% Calculate perimeter of each section
```

```
vv=F(N,T);
yl=[-3.1416;3.1416];
xl=[xx(722);xx(722)];
xl2=[xx(1084);xx(1084)];
xl3=[xx(1360);xx(1360)];
[yc.a,zc.a]=pol2cart(tu,vv(:,722));
[yc.b,zc.b]=pol2cart(tu,vv(:,1084));
[yc.c,zc.c]=pol2cart(tu,vv(:,1360));
```

```
vv=F(N,T);
yl=[-3.1416;3.1416];
xl=[xx(250);xx(250)];
xl2=[xx(860);xx(860)];
xl3=[xx(1004);xx(1004)];
[yc.a,zc.a]=pol2cart(tu,vv(:,250));
[yc.b,zc.b]=pol2cart(tu,vv(:,860));
[yc.c,zc.c]=pol2cart(tu,vv(:,1004));
```

```
vv=F(N,T);
yl=[-3.1416;3.1416];
xl=[xx(1010);xx(1010)];
xl2=[xx(1257);xx(1257)];
xl3=[xx(1334);xx(1334)];
[yc.a,zc.a]=pol2cart(tu,vv(:,1010));
[yc.b,zc.b]=pol2cart(tu,vv(:,1257));
[yc.c,zc.c]=pol2cart(tu,vv(:,1334));
```

```
vv=F(N,T);
yl=[-3.1416;3.1416];
xl=[xx(1209);xx(1209)];
xl2=[xx(1584);xx(1584)];
xl3=[xx(1958);xx(1958)];
[yc.a,zc.a]=pol2cart(tu,vv(:,1209));
[yc.b,zc.b]=pol2cart(tu,vv(:,1584));
[yc.c,zc.c]=pol2cart(tu,vv(:,1958));
```

```
vv=F(N,T);
yl=[-3.1416;3.1416];
xl=[xx(179);xx(179)];
xl2=[xx(717);xx(717)];
xl3=[xx(1001);xx(1001)];
[yc.a,zc.a]=pol2cart(tu,vv(:,179));
[yc.b,zc.b]=pol2cart(tu,vv(:,717));
[yc.c,zc.c]=pol2cart(tu,vv(:,1001));
```

```
[N,T] = meshgrid(xx,tu);

vv=F(N,T);
yl=[-3.1416;3.1416];
xl=[xx(1271);xx(1271)];
xl2=[xx(1459);xx(1459)];
xl3=[xx(1751);xx(1751)];
[yc.a,zc.a]=pol2cart(tu,vv(:,1271));
[yc.b,zc.b]=pol2cart(tu,vv(:,1459));
[yc.c,zc.c]=pol2cart(tu,vv(:,1751));
```

```
vv=F(N,T);
yl=[-3.1416;3.1416];
xl=[xx(1251);xx(1251)];
xl2=[xx(1334);xx(1334)];
xl3=[xx(1442);xx(1442)];
[yc.a,zc.a]=pol2cart(tu,vv(:,1251));
[yc.b,zc.b]=pol2cart(tu,vv(:,1334));
[yc.c,zc.c]=pol2cart(tu,vv(:,1442));
```

```
vv=F(N,T);
yl=[-3.1416;3.1416];
xl=[xx(1458);xx(1458)];
xl2=[xx(1517);xx(1517)];
xl3=[xx(1570);xx(1570)];
[yc.a,zc.a]=pol2cart(tu,vv(:,1458));
[yc.b,zc.b]=pol2cart(tu,vv(:,1517));
[yc.c,zc.c]=pol2cart(tu,vv(:,1570));
```

```
vv=F(N,T);
yl=[-3.1416;3.1416];
xl=[xx(1);xx(1)];
xl2=[xx(396);xx(396)];
xl3=[xx(1470);xx(1470)];
[yc.a,zc.a]=pol2cart(tu,vv(:,1));
[yc.b,zc.b]=pol2cart(tu,vv(:,396));
[yc.c,zc.c]=pol2cart(tu,vv(:,1470));
```

```
vv=F(N,T);
yl=[-3.1416;3.1416];
xl=[xx(1084);xx(1084)];
xl2=[xx(1364);xx(1364)];
xl3=[xx(1584);xx(1584)];
[yc.a,zc.a]=pol2cart(tu,vv(:,1084));
[yc.b,zc.b]=pol2cart(tu,vv(:,1364));
[yc.c,zc.c]=pol2cart(tu,vv(:,1584));
```

```
vv=F(N,T);
yl=[-3.1416;3.1416];
xl=[xx(1124);xx(1124)];
xl2=[xx(1160);xx(1160)];
xl3=[xx(1334);xx(1334)];
[yc.a,zc.a]=pol2cart(tu,vv(:,1124));
[yc.b,zc.b]=pol2cart(tu,vv(:,1160));
[yc.c,zc.c]=pol2cart(tu,vv(:,1334));


vv=F(N,T);
yl=[-3.1416;3.1416];
xl=[xx(606);xx(606)];
xl2=[xx(1084);xx(1084)];
xl3=[xx(1376);xx(1376)];
[yc.a,zc.a]=pol2cart(tu,vv(:,606));
[yc.b,zc.b]=pol2cart(tu,vv(:,1084));
[yc.c,zc.c]=pol2cart(tu,vv(:,1376));


vv=F(N,T);
yl=[-3.1416;3.1416];
xl=[xx(875);xx(875)];
xl2=[xx(1088);xx(1088)];
xl3=[xx(1547);xx(1547)];
[yc.a,zc.a]=pol2cart(tu,vv(:,875));
[yc.b,zc.b]=pol2cart(tu,vv(:,1088));
[yc.c,zc.c]=pol2cart(tu,vv(:,1547));
%set here the average uncorroded area

vv=F(N,T);
yl=[-3.1416;3.1416];
xl=[xx(546);xx(546)];
xl2=[xx(1238);xx(1238)];
xl3=[xx(2000);xx(2000)];
[yc.a,zc.a]=pol2cart(tu,vv(:,546));
[yc.b,zc.b]=pol2cart(tu,vv(:,1238));
[yc.c,zc.c]=pol2cart(tu,vv(:,2000));
%set here the average uncorroded area


vv=F(N,T);
yl=[-3.1416;3.1416];
xl=[xx(188);xx(188)];
xl2=[xx(688);xx(688)];
xl3=[xx(1327);xx(1327)];
[yc.a,zc.a]=pol2cart(tu,vv(:,188));
[yc.b,zc.b]=pol2cart(tu,vv(:,688));
[yc.c,zc.c]=pol2cart(tu,vv(:,1327));
%set here the average uncorroded area
```

```
vv=F(N,T);
yl=[-3.1416;3.1416];
xl=[xx(500);xx(500)];
xl2=[xx(1001);xx(1001)];
xl3=[xx(1188);xx(1188)];
[yc.a,zc.a]=pol2cart(tu,vv(:,500));
[yc.b,zc.b]=pol2cart(tu,vv(:,1001));
[yc.c,zc.c]=pol2cart(tu,vv(:,1188));

vv=F(N,T);
yl=[-3.1416;3.1416];
xl=[xx(1313);xx(1313)];
xl2=[xx(1501);xx(1501)];
xl3=[xx(1800);xx(1800)];
[yc.a,zc.a]=pol2cart(tu,vv(:,1313));
[yc.b,zc.b]=pol2cart(tu,vv(:,1501));
[yc.c,zc.c]=pol2cart(tu,vv(:,1800));
%set here the average uncorroded area


vv=F(N,T);
yl=[-3.1416;3.1416];
xl=[xx(1);xx(1)];
xl2=[xx(662);xx(662)];
xl3=[xx(1063);xx(1063)];
[yc.a,zc.a]=pol2cart(tu,vv(:,1));
[yc.b,zc.b]=pol2cart(tu,vv(:,662));
[yc.c,zc.c]=pol2cart(tu,vv(:,1063));
%set here the average uncorroded area


vv=F(N,T);
yl=[-3.1416;3.1416];
xl=[xx(488);xx(488)];
xl2=[xx(1157);xx(1157)];
xl3=[xx(1376);xx(1376)];
[yc.a,zc.a]=pol2cart(tu,vv(:,488));
[yc.b,zc.b]=pol2cart(tu,vv(:,1157));
[yc.c,zc.c]=pol2cart(tu,vv(:,1376));
%set here the average uncorroded area


vv=F(N,T);
yl=[-3.1416;3.1416];
xl=[xx(365);xx(365)];
xl2=[xx(1626);xx(1626)];
xl3=[xx(2000);xx(2000)];
[yc.a,zc.a]=pol2cart(tu,vv(:,365));
[yc.b,zc.b]=pol2cart(tu,vv(:,1626));
[yc.c,zc.c]=pol2cart(tu,vv(:,2000));
%set here the average uncorroded area
```

```
vv=F(N,T);
yl=[-3.1416;3.1416];
xl=[xx(437);xx(437)];
xl2=[xx(738);xx(738)];
xl3=[xx(2000);xx(2000)];
[yc.a,zc.a]=pol2cart(tu,vv(:,437));
[yc.b,zc.b]=pol2cart(tu,vv(:,738));
[yc.c,zc.c]=pol2cart(tu,vv(:,2000));
%set here the average uncorroded area
```

```
vv=F(N,T);
yl=[-3.1416;3.1416];
xl=[xx(238);xx(238)];
xl2=[xx(1601);xx(1601)];
xl3=[xx(2000);xx(2000)];
[yc.a,zc.a]=pol2cart(tu,vv(:,238));
[yc.b,zc.b]=pol2cart(tu,vv(:,1601));
[yc.c,zc.c]=pol2cart(tu,vv(:,2000));
%set here the average uncorroded area
```

```
vv=F(N,T);
yl=[-3.1416;3.1416];
xl=[xx(1051);xx(1051)];
xl2=[xx(1351);xx(1351)];
xl3=[xx(1938);xx(1938)];
[yc.a,zc.a]=pol2cart(tu,vv(:,1051));
[yc.b,zc.b]=pol2cart(tu,vv(:,1351));
[yc.c,zc.c]=pol2cart(tu,vv(:,1938));
%set here the average uncorroded area
```

```
vv=F(N,T);
yl=[-3.1416;3.1416];
xl=[xx(1);xx(1)];
xl2=[xx(150);xx(150)];
xl3=[xx(500);xx(500)];
[yc.a,zc.a]=pol2cart(tu,vv(:,1));
[yc.b,zc.b]=pol2cart(tu,vv(:,150));
[yc.c,zc.c]=pol2cart(tu,vv(:,500));
%set here the average uncorroded area
```

```
vv=F(N,T);
yl=[-3.1416;3.1416];
xl=[xx(487);xx(487)];
xl2=[xx(1088);xx(1088)];
xl3=[xx(1488);xx(1488)];
[yc.a,zc.a]=pol2cart(tu,vv(:,487));
[yc.b,zc.b]=pol2cart(tu,vv(:,1088));
[yc.c,zc.c]=pol2cart(tu,vv(:,1488));
%set here the average uncorroded area
```

```
vv=F(N,T);
yl=[-3.1416;3.1416];
xl=[xx(336);xx(336)];
xl2=[xx(1101);xx(1101)];
xl3=[xx(1563);xx(1563)];
[yc.a,zc.a]=pol2cart(tu,vv(:,336));
[yc.b,zc.b]=pol2cart(tu,vv(:,1101));
[yc.c,zc.c]=pol2cart(tu,vv(:,1563));
%set here the average uncorroded area
```

```
vv=F(N,T);
yl=[-3.1416;3.1416];
xl=[xx(688);xx(688)];
xl2=[xx(1131);xx(1131)];
xl3=[xx(1838);xx(1838)];
[yc.a,zc.a]=pol2cart(tu,vv(:,688));
[yc.b,zc.b]=pol2cart(tu,vv(:,1131));
[yc.c,zc.c]=pol2cart(tu,vv(:,1838));
%set here the average uncorroded area
```

```
vv=F(N,T);
yl=[-3.1416;3.1416];
xl=[xx(1001);xx(1001)];
xl2=[xx(1576);xx(1576)];
xl3=[xx(1776);xx(1776)];
[yc.a,zc.a]=pol2cart(tu,vv(:,1001));
[yc.b,zc.b]=pol2cart(tu,vv(:,1576));
[yc.c,zc.c]=pol2cart(tu,vv(:,1776));
%set here the average uncorroded area
```

```
vv=F(N,T);
yl=[-3.1416;3.1416];
xl=[xx(470);xx(470)];
xl2=[xx(1526);xx(1526)];
xl3=[xx(2000);xx(2000)];
[yc.a,zc.a]=pol2cart(tu,vv(:,470));
[yc.b,zc.b]=pol2cart(tu,vv(:,1526));
[yc.c,zc.c]=pol2cart(tu,vv(:,2000));
%set here the average uncorroded area
```

```
vv=F(N,T);
yl=[-3.1416;3.1416];
xl=[xx(125);xx(125)];
xl2=[xx(1225);xx(1225)];
xl3=[xx(1688);xx(1688)];
[yc.a,zc.a]=pol2cart(tu,vv(:,125));
[yc.b,zc.b]=pol2cart(tu,vv(:,1225));
[yc.c,zc.c]=pol2cart(tu,vv(:,1688));
%set here the average uncorroded area
```

```
vv=F(N,T);
yl=[-3.1416;3.1416];
xl=[xx(599);xx(599)];
xl2=[xx(1501);xx(1501)];
xl3=[xx(2000);xx(2000)];
[yc.a,zc.a]=pol2cart(tu,vv(:,599));
[yc.b,zc.b]=pol2cart(tu,vv(:,1501));
[yc.c,zc.c]=pol2cart(tu,vv(:,2000));
%set here the average uncorroded area
```

DEPARTMENT OF ARCHITECTURE AND
CIVIL ENGINEERING
CHALMERS UNIVERSITY OF TECHNOLOGY
Gothenburg, Sweden 2025
www.chalmers.se

CHALMERS
UNIVERSITY OF TECHNOLOGY